

Effects of light scalar mesons in a
soliton model for the nucleon
核子に対するソリトン模型におけ
る軽いスカラー中間子の効果

何秉然

Department of Physics, Nagoya University

February, 2016

Abstract

The investigation of the properties of baryons in low energy regions is an important issue in hadron physics. The Skyrme model provides a systematic way to investigate baryon properties through meson dynamics. In low energy regions, meson dynamics are well described by several effective theories, e.g., chiral perturbation theory (ChPT) and hidden local symmetry (HLS). The Lagrangian of an original Skyrme model is a particular choice of ChPT. To construct a baryon state from low energy constants, rho and omega mesons are also included within the framework of HLS. However, the mass of a skyrmion obtained from HLS is approximately 50% heavier than the lightest baryon. Later, it was observed that including a dilaton-type scalar meson provides an attractive force, which drops the mass of the skyrmion.

In this thesis, we study the effects of light scalar mesons on skyrmion properties. As an extension of HLS, we construct a mesonic model that includes two-quark and four-quark scalar meson fields.

First, we switch off the four-quark scalar meson field. We then have two model parameters: (i) the mass of the two-quark scalar meson field and (ii) the coupling strength between the two-quark scalar and vector meson fields. On keeping the coupling strength constant, we observe that the skyrmion mass decreases and the skyrmion size increases when the mass of the scalar meson decreases. On keeping the mass of the two-quark scalar meson field constant, we observe that the skyrmion mass and baryon number density increase as the coupling strength increases. Finally, we switch on the four-quark scalar meson field and investigate the mixing of skyrmion properties between the two-quark and four-quark scalar mesons. We observe that when the light scalar meson includes more of the two-quark component, the skyrmion mass becomes lighter and its size becomes larger.

Contents

1	Introduction	1
2	QCD and its properties	5
2.1	Symmetry and Conserved Current	5
2.2	QCD Lagrangian	7
2.3	Chirality and Chiral Symmetry	8
2.4	Spontaneous Symmetry Breaking	9
3	Effective Lagrangian for mesons in the low energy region	11
3.1	Chiral perturbation theory	11
3.1.1	Lowest order effective Lagrangian	11
3.1.2	Spontaneously symmetry breaking by the quark masses	13
3.1.3	General Lagrangian	14
3.2	Hidden local symmetry	16
3.2.1	$G_{\text{global}} \times H_{\text{local}}$ symmetry	16
3.2.2	General Lagrangian	18
3.2.3	Relations between HLS and ChPT	19
4	Skyrme model	20
4.1	Skyrme model with the pion	20
4.1.1	The model	20
4.1.2	Quantize the skyrmion	22
4.2	Skyrme model with π , ρ , and ω mesons	24
4.2.1	The model	25
4.2.2	Collective quantization of the skyrmion	26
4.3	Skyrme model with light scalar mesons	27
4.3.1	The model	27
4.3.2	The ansatz	31
4.3.3	Effects of scalar mesons when $A = 0$	33
4.3.4	Effects of scalar mesons when $A \neq 0$	36

	II
5 Discussion and Conclusion	39
Acknowledgements	41
A The mass mixing matrix for the scalar meson	42
B Skyrmion mass and the equations of motion for the profile functions <i>F(r), G(r), W(r), $\bar{\sigma}(r)$, and $\bar{\phi}(r)$</i>	43

List of Figures

1.1	QCD phase diagram	2
2.1	The mechanism of spontaneously symmetry breaking	10
4.1	Hedgehog ansatz	22
4.2	Profile function for $F(r)$	23
4.3	m_σ dependence of the skyrmion mass and radii with $A = s_0 = 0$.	34
4.4	m_σ dependence of the profile functions with $A = s_0 = 0$ for $m_\sigma = 1$ GeV (green curve) and $m_\sigma = 1.4$ GeV (red dash-dotted line)	34
4.5	s_0 dependence of the skyrmion mass and radii for $m_\sigma = 1.37$ GeV	36
4.6	Profile functions with $s_0 = -0.5$ (green curve) and $s_0 = 0$ (red dash-dotted line)	37
4.7	Dependence of skyrmion properties on the mixing angle between two scalar mesons for $s_0 = 0$	38
4.8	Dependence of skyrmion properties on the mixing angle between two scalar mesons for $s_0 = -0.5$	38

List of Tables

1.1	The mass and radius of skyrmions from the π and $\pi\rho\omega$ models . .	3
1.2	Mass and radius of the skyrmion from the $\pi\sigma$ and $\pi\rho\omega\chi$ models .	3
2.1	Symmetry and corresponding conserved quantity	5
3.1	Transformation properties of the ChPT operators	14
3.2	Transformation properties of HLS operators	18
4.1	Inputs and predictions of the quantized skyrmion	25
4.2	Inputs and predictions of the collective quantized skyrmion when $a_{\text{hls}} = 2$	27
4.3	Parameters of the model	33
5.1	The parameter dependence of mass and radius of the skyrmion (\diamond 's denote the previous analysis and \blacklozenge 's denote the present anal- ysis.)	40
5.2	The mass and radius of the skyrmion from the leading order (\diamond 's denote the previous analysis and \blacklozenge denotes the present analysis) .	40
5.3	The mass and radius of the skyrmion from the $\mathcal{O}(p^4)$ terms of HLS	40

Chapter 1

Introduction

Quantum chromodynamics (QCD) is a fundamental theory that describes the dynamics of quarks and gluons. There are two important features of QCD: (i) quark confinement and (ii) asymptotic freedom. These two features make it difficult to perform a perturbative calculation of QCD dynamics in a low energy region. Therefore, instead of using QCD, many effective theories have been developed to probe meson and baryon dynamics in this region. For example, chiral perturbation theory and hidden local symmetry are widely used to describe meson dynamics, whereas the Skyrme model, the Massachusetts Institute of Technology (MIT) bag model, and the chiral bag model are widely used to describe baryon dynamics.

In the real world, some extreme conditions exist, e.g., high temperature and high density. Figure 1.1 shows a phase diagram of a quark-gluon system in the temperature-density plane (for review articles, see, e.g., ^[1-4]). At zero density, lattice QCD is a powerful method to investigate the QCD dynamics. For example, lattice calculations^[5;6] show that as the temperature increases, there is a phase transition between the hadronic phase and the quark-gluon-plasma phase. However, in the finite density region, lattice QCD is not an effective way to study QCD properties because of the ‘sign’ problem. Therefore, great efforts have been made to investigate the QCD dynamics in the dense region by using several effective models^[7-9].

In the very-high-density region, the baryons overlap each other; therefore, the size effect of the baryon plays an important role when studying QCD dynamics. There are several models that include the effect of baryon size, e.g., soliton models, the MIT bag model, and the chiral bag model. In this thesis, we focus on soliton models, because they provide a systematic way to investigate the density effect of QCD^[10;11].

In 1962, T. H. R. Skyrme proposed the idea that a baryon could be identified as a soliton solution of the mesonic theory^[12]. Because this idea was originally

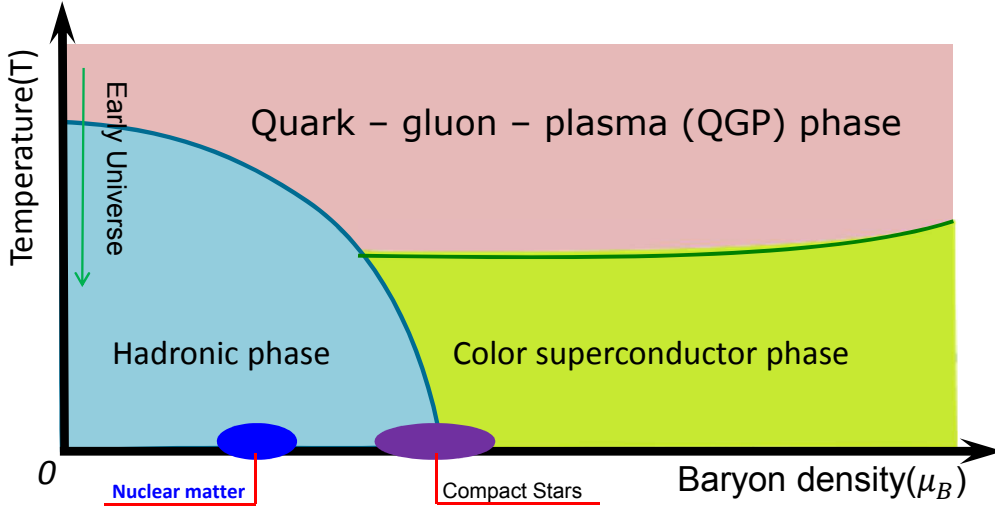


Figure 1.1: QCD phase diagram

proposed by Skyrme, soliton models are generally called Skyrme models, and the soliton solution is called the skyrmion. Since then, this idea has been widely applied in condensed matter, nuclear, and particle physics^[13]. In the original Skyrme model, where only the pion was considered, it was found that if we impose the parameters from the pion properties, the Skyrme baryon is approximately twice as heavy as the nucleon.

To reproduce the baryon properties consistently with the mesonic model, the rho meson is introduced within the framework of HLS^[14–16]. Inclusion of the vector meson generates a repulsive force, which stabilizes the soliton, and the baryon mass and size become closer to the experimental values than those obtained in the model including only the pion. Because the omega meson has a similar mass and plays a similar role as the rho meson does, the omega meson is also introduced. However, the repulsive force from the vector mesons is too strong, which makes the skyrmion obtained from the HLS model approximately 50% heavier than the nucleon^[17;18]. The experimental values and model predictions of the mass and radius of solitons from the π and $\pi\rho\omega$ models are summarized in Table 1.1.

The scalar meson is expected to generate an attractive force, which balances the repulsive force generated by vector mesons. As a result, the incorporation of a scalar meson reduces the mass of a soliton. So far, in the Skyrme approach, scalar mesons are introduced in two ways: (i) as the chiral partner of the pion, i.e., a scalar meson made from two quarks^[19] and (ii) as the Nambu-Goldstone (NG) boson of the scale symmetry, i.e., the dilaton^[20–25]. It is observed that scalar

Table 1.1: The mass and radius of skyrmions from the π and $\pi\rho\omega$ models

model	soliton mass [MeV]	$\sqrt{\langle r^2 \rangle_B}$ [fm]
π ^[19]	1756.5	0.51
$\pi\rho\omega$ ^[20]	1469.0	0.49
Experiment	939	0.72

mesons provide an attractive force and reduce skyrmion mass as shown in Table 1.2.

Table 1.2: Mass and radius of the skyrmion from the $\pi\sigma$ and $\pi\rho\omega\chi$ models

model	scalar type	soliton mass [MeV]	$\sqrt{\langle r^2 \rangle_B}$ [fm]
$\pi\sigma$ ^[19]	2 quark	1364.5	0.56
$\pi\rho\omega\chi$ ^[20]	glueball	1408.3	0.51

Comparing Tables 1.2 and 1.1, we observe that the scalar mesons play important roles to reproduce the mass and radius of the light nucleons. However, the scalar meson made from two quarks is a p -wave state in the quark model and its mass is approximately 1.3 GeV. Instead, several studies suggest that the scalar mesons made from two quarks mix with those from four quarks^[26;27]. Furthermore, the light glueball mass^[20] is not consistent with Lattice predictions. Thus, following^[27], we consider light scalar mesons as mixing states of two-quark and four-quark states.

In this thesis, we investigate the effect of scalar mesons on the mass and size of a skyrmion. The model is constructed as a chiral effective model, which includes the pion, rho, and omega mesons together with two-quark and four-quark scalar mesons. In the present study, the parameters of the model are determined through low energy experiment results.

Our findings are summarized as follows:

1. When we switch off the mixing between the two-quark and four-quark scalar mesons, the four-quark component scalar state decouples from the model; therefore, the scalar meson is a pure two-quark state. In such a case, we find that:
 - (a) The skyrmion mass depends on the mass of the scalar meson; with increasing scalar meson mass, the skyrmion mass and size decrease.
 - (b) The skyrmion mass depends on the coupling strength between the scalar meson and the vector mesons. Thus, with an increasing coupling strength, both the skyrmion mass and the charge radius of the baryon number density increase.

2. When we switch on the mixing between the two-quark and four-quark scalar mesons, the mixing strength affects skyrmion properties. When the two-quark component of the lighter scalar meson is increased, the skyrmion mass becomes smaller and its size larger.

This thesis is organized as follows. In Ch. 2, we introduce, briefly, the basics of QCD, chiral symmetry, and chiral symmetry breaking. In Ch. 3, we briefly review the effective theories of QCD in the low energy region, i.e., the fundamental concepts and properties of ChPT and HLS. In Ch. 4, we review the Skyrme model including the pion, rho, and omega mesons. In Sec. 4.3, we include the scalar meson in the theory and analyze, numerically, the effects of scalar mesons on skyrmion properties. In Ch. 5, we give a brief summary. Some details of the calculations are given in the Appendices.

Chapter 2

QCD and its properties

In hadron physics, the fundamental elements are quarks and gluons. The gluons carry color charge and both quarks and gluons interact through the exchange of gluons. The theory that describes this dynamics is QCD. The strong interaction (color force) of the quarks and gluons make up hadrons (such as the proton, neutron, and pion). QCD is an important part of the Standard Model of particle physics and experimental evidence for QCD has been gathered over several decades.

2.1 Symmetry and Conserved Current

In this section, we describe the relation between the symmetry and the conserved quantities.

In nature, a physical system has a symmetry when the physical laws of the system remain unchanged after a transformation. Noether's theorem states that when the system has a continuous symmetry, there exists a corresponding conserved quantity.

Table 2.1: Symmetry and corresponding conserved quantity

invariance	conserved quantity
translation in time	energy
translation in space	momentum
rotation in space	angular momentum
coordinate inversion	spatial parity
time reversal	time reversal
charge conjugation	charge parity

For example, when the system is invariant under time translation, the energy

of the system is conserved. The momentum of the system is conserved when the system is invariant under a space translation. Table 2.1 shows some symmetries and the corresponding conserved quantities.

In the low energy region, mesons play a more important role than free quarks do. The bilinear representation of the Dirac spinor is introduced as

$$S(x) = \bar{\psi}(x)\psi(x), \quad (2.1)$$

$$V^\mu(x) = \bar{\psi}(x)\gamma^\mu\psi(x), \quad (2.2)$$

$$A^\mu(x) = \bar{\psi}(x)\gamma^\mu\gamma_5\psi(x), \quad (2.3)$$

where μ is the Lorentz index with $\mu \in (0, 1, 2, 3)$, $\bar{\psi}(x) = \psi^\dagger\gamma^0$, and γ^μ denotes the gamma matrices, which are expressed as

$$\gamma^0 = \begin{pmatrix} \mathbb{1} & 0 \\ 0 & \mathbb{1} \end{pmatrix}, \quad \vec{\gamma} = \begin{pmatrix} 0 & \vec{\tau} \\ -\vec{\tau} & 0 \end{pmatrix}, \quad \gamma_5 = \gamma^5 \equiv i\gamma_0\gamma_1\gamma_2\gamma_3 = \begin{pmatrix} 0 & \mathbb{1} \\ \mathbb{1} & 0 \end{pmatrix}. \quad (2.4)$$

Here $\mathbb{1}$ and σ are the rank-2 unit matrix and Pauli matrices, respectively. The latter are expressed as

$$\mathbb{1} = \begin{pmatrix} 1 & 0 \\ 0 & 1 \end{pmatrix}, \quad \tau_x = \begin{pmatrix} 0 & 1 \\ 1 & 0 \end{pmatrix}, \quad \tau_y = \begin{pmatrix} 0 & -i \\ i & 0 \end{pmatrix}, \quad \tau_z = \begin{pmatrix} 1 & 0 \\ 0 & -1 \end{pmatrix}. \quad (2.5)$$

Under the Lorentz transformation, S , V , and A transforms similarly as a scalar, vector, and axial vector, respectively. The time component of Eq. (2.2) is expressed as

$$V^0(x) = \bar{\psi}(x)\gamma^0\psi(x) = \psi(x)^\dagger\psi(x), \quad (2.6)$$

which corresponds to the quark number density.

The left- and right-handed currents are

$$A_L^\mu(x) = \bar{\psi}_L(x)\gamma^\mu\psi_L(x) = \frac{1}{2}(V^\mu + A^\mu), \quad (2.7)$$

$$A_R^\mu(x) = \bar{\psi}_R(x)\gamma^\mu\psi_R(x) = \frac{1}{2}(V^\mu - A^\mu). \quad (2.8)$$

The Lagrangian of the free Dirac particles is written as

$$\bar{\psi}(i\partial^\mu\gamma_\mu - m)\psi. \quad (2.9)$$

Under the axial vector transformation, ψ transform as $\psi \xrightarrow{\text{axial}} \exp(i\vec{t} \cdot \vec{\theta}_A\gamma_5)\psi$, where $\vec{\theta}_A = (\vec{\theta}_L - \vec{\theta}_R)$ is an isospin transformation parameter, and \vec{t} is the group generator corresponding to $\vec{\theta}_A$. The mass term of the Dirac fields transforms in the manner

$$m\bar{\psi}\psi \xrightarrow{\text{axial}} m\psi^\dagger \exp(-i\vec{t} \cdot \vec{\theta}_A\gamma_5^\dagger)\gamma^0 \exp(i\vec{t} \cdot \vec{\theta}_A\gamma_5)\psi$$

$$= m\bar{\psi} \exp(2i\vec{t} \cdot \vec{\theta}_A \gamma_5) \psi. \quad (2.10)$$

If $m \neq 0$, we observe that the mass term is not invariant under the axial vector transformation. Therefore, the non-vanishing mass of the Dirac particle breaks the chiral symmetry. We will discuss more regarding the relation between the Dirac mass and chiral symmetry later.

2.2 QCD Lagrangian

The QCD Lagrangian is written as

$$\mathcal{L} = \bar{\psi}(i\gamma_\mu D^\mu - m)\psi - \frac{1}{2} \text{Tr} G_{\mu\nu} G^{\mu\nu}, \quad (2.11)$$

where $\psi = (\psi_{\alpha i})$ denote the quark fields, α is the flavor index with $\alpha \in (u, d, s, c, b, t)$, and i is the color index with $i \in (1, 2, 3)$. Here, $G_{\mu\nu}$ denotes the gluon field tensor, which is expressed as

$$G_{\mu\nu} \equiv G_{\mu\nu}^a t_a \equiv (\partial_\mu A_\nu^a - \partial_\nu A_\mu^a + g f_{abc} A_\mu^b A_\nu^c) t_a, \quad (2.12)$$

where g is a gauge coupling constant, $A_\mu^a(x)$ are the gauge fields of the ‘‘gluon’’, t_a is the generator of $SU(N_c)_c$, and N_c is the number of colors. When $N_c = 3$, a satisfies $a \in (1, 2, 3 \dots, 8)$. m is the quark mass matrix, which is expressed as

$$m = \text{diag}(m_u, m_d, m_s, m_c, m_b, m_t). \quad (2.13)$$

f_{abc} is the structure constant, which is expressed as

$$f_{abc} = -i \text{Tr} \left(\left[\frac{t_a}{2}, \frac{t_b}{2} \right] t_c \right). \quad (2.14)$$

For the $N_c = 3$ case, the non-vanishing f_{abc} are expressed as

$$\begin{aligned} f_{123} &= 1, \\ f_{147} &= -f_{156} = f_{246} = f_{257} = f_{345} = -f_{367} = \frac{1}{2}, \\ f_{458} &= f_{678} = \sqrt{\frac{3}{2}}. \end{aligned} \quad (2.15)$$

Note that $\psi_{\alpha i}$ is a 4-component Dirac spinor with the number of flavors $N_f = 6$ and the number of colors $N_c = 3$.

The gauge-covariant derivative is expressed as

$$D_\mu = \partial_\mu - igA_\mu(x), \quad (2.16)$$

where

$$A_\mu(x) = \sum_{a=1}^8 t_a A_\mu^a(x). \quad (2.17)$$

The physics of the strong interaction of the quarks is invariant under the gauge transformation, i.e.,

$$\psi(x) \xrightarrow{\text{gauge}} \tilde{\psi}(x) = U\psi(x), \quad (2.18)$$

where $U = \exp[-i\theta_a(x)t_a]$ and $\theta_a(x)$ is a real function.

The infinitesimal gauge transformation for (2.18) is expressed as

$$U = \exp[-i\theta_a(x)t_a] = 1 - i\theta_a(x)t_a + \mathcal{O}(\theta^2). \quad (2.19)$$

Up to terms linear in $\theta_a(x)$, the transformation of the gauge field is

$$A_a^\mu(x) \xrightarrow{\text{gauge}} \tilde{A}_a^\mu(x) = A_a^\mu(x) - \frac{1}{g}\partial_\mu\theta_a(x) + f_{abc}\theta_b(x)A_c^\mu(x). \quad (2.20)$$

2.3 Chirality and Chiral Symmetry

If the quark mass is negligible, i.e., $m_q \sim 0$, the Lagrangian (2.11) can be rewritten as

$$\mathcal{L} = \bar{\psi}(i\gamma_\mu D^\mu)\psi - \frac{1}{2}\text{Tr} G_{\mu\nu}G^{\mu\nu}. \quad (2.21)$$

In this case, the left- and right-handed quark fields are decoupled as

$$\begin{aligned} \mathcal{L} &= \bar{\psi}(i\gamma_\mu D^\mu)\psi - \frac{1}{2}\text{Tr} G_{\mu\nu}G^{\mu\nu} \\ &= \bar{\psi}_L i\gamma_\mu D^\mu \psi_L + \bar{\psi}_R i\gamma_\mu D^\mu \psi_R - \frac{1}{2}\text{Tr} G_{\mu\nu}G^{\mu\nu}, \end{aligned} \quad (2.22)$$

where ψ_L and ψ_R denote the left- and right-handed quarks, respectively. They are defined as

$$\psi_L = \frac{1 + \gamma^5}{2}\psi, \quad (2.23)$$

$$\psi_R = \frac{1 - \gamma^5}{2}\psi. \quad (2.24)$$

The projector relations for ψ_L and ψ_R are

$$\psi_L = \gamma^5\psi_L, \quad (2.25)$$

$$\psi_R = -\gamma^5\psi_R. \quad (2.26)$$

The chiral transformations for ψ_L and ψ_R are

$$\psi_L \xrightarrow{\text{chiral}} \exp(i\vec{t} \cdot \vec{\theta}_L) \psi_L, \quad \psi_R \xrightarrow{\text{chiral}} \exp(i\vec{t} \cdot \vec{\theta}_R) \psi_R. \quad (2.27)$$

Under the chiral transformation, the first term in Eq. (2.22),

$$\begin{aligned} \bar{\psi}_L i\gamma_\mu D^\mu \psi_L &\xrightarrow{\text{chiral}} \psi_L^\dagger \exp(-i\vec{t} \cdot \vec{\theta}_L) \gamma^0 i\gamma_\mu D^\mu \exp(i\vec{t} \cdot \vec{\theta}_L) \psi_L \\ &= \bar{\psi}_L i\gamma_\mu D^\mu \psi_L, \end{aligned} \quad (2.28)$$

is chiral invariant. Similarly, we can show that the second term in Eq. (2.22) is also chiral invariant. Therefore, when $m_q \sim 0$, the Lagrangian (2.11) is invariant under a chiral transformation with separated left- and right-handed pieces. This is called chiral symmetry.

2.4 Spontaneous Symmetry Breaking

When we look at the meson and baryon masses, we find that they are much bigger than the current quark masses. For example, the nucleon mass is roughly 940 MeV, but the current masses are 2.3 and 4.8 MeV for the u and d quarks, respectively. One possible origin of the mass generation is that the meson and the baryon masses are dynamically generated from spontaneous chiral symmetry breaking given as^[28]

$$SU(N_f)_L \times SU(N_f)_R \rightarrow SU(N_f)_V, \quad (2.29)$$

where the number of flavors $N_f \leq 3$. When the meson and baryon masses are derived from the vacuum expectation value (VEV) of the scalar particle, like in the Higgs mechanism, the shift of the vacuum value away from zero provides masses for the meson and baryons. This non-vanishing value of VEV of the scalar particle breaks the chiral symmetry and only the isospin symmetry remains in the vacuum. In this scenario, we expect that the baryon and meson masses will vanish when we approach the chiral restoration point. The restoration of the chiral symmetry and the degeneration of the baryon and meson masses are discussed in many papers^[29–31].

The concept of spontaneous chiral symmetry breaking is discussed in the Nambu-Jona-Lasinio (NJL) model^[32]. For a review of the NJL model, please see^[33]. A lattice QCD calculation shows that chiral symmetry is spontaneously broken in vacuum^[34].

To estimate the mechanism of spontaneously symmetry breaking, we show several types of potentials in Fig. 2.1. There are three patterns: (a) a stable vacuum at the origin, (b) a stable vacuum on the circle around the origin, and (c) a stable vacuum, which is located on the x -axis.

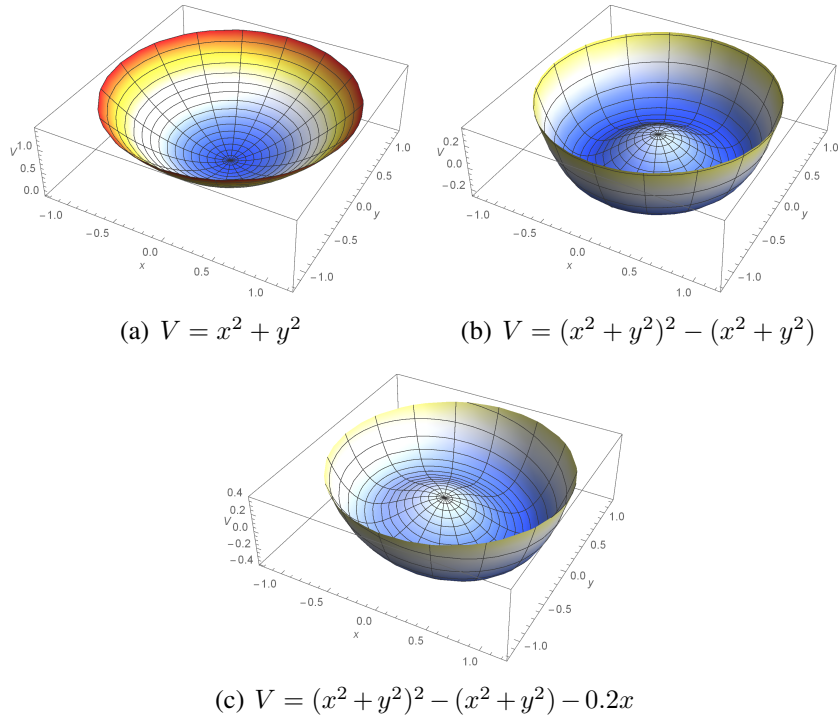


Figure 2.1: The mechanism of spontaneously symmetry breaking

For QCD, there are two types of signatures that indicate that chiral symmetry is spontaneously broken: (i) $\langle \bar{q}q \rangle \neq 0$ (sufficient but not necessary condition) and (ii) $f_\pi \neq 0$ (sufficient and necessary condition). Here, f_π is the pion decay constant, which is defined by

$$\langle 0 | A_a^\mu(0) | \pi_b(p) \rangle = -i p^\mu f_\pi \delta_{ab}. \quad (2.30)$$

In the following sections, we will discuss the chiral-symmetry-breaking pattern more explicitly.

Chapter 3

Effective Lagrangian for mesons in the low energy region

3.1 Chiral perturbation theory

For a certain energy scale Λ , the heavy degrees of freedoms are integrated out while the light degrees of freedoms remain. Below the scale of spontaneous chiral symmetry breaking, ChPT is a powerful and well-accepted method^[35–38]. ChPT is based on the fact that for energies below 1 GeV, the relevant degrees of freedom of QCD are not the quarks and gluons, but the mesons. Because the pion is the lightest pseudoscalar meson, it is treated as the dynamical field in the ChPT approach. The meson fields that are heavier than the pion, e.g., the vector and scalar mesons, are treated as external fields. In the following subsections, we briefly introduce the concepts of ChPT following Refs.^[35–41].

3.1.1 Lowest order effective Lagrangian

We start by constructing the lowest order effective Lagrangian for the lightest meson state. We limit the number of quark flavors to $N_f = 2$, with the pion as the corresponding NG boson. The pion field is written as

$$\pi = \sum_{i=1}^3 \phi_i \frac{\tau_i}{2} = \frac{1}{2} \begin{pmatrix} \pi^0 & \sqrt{2}\pi^+ \\ \sqrt{2}\pi^- & -\pi^0 \end{pmatrix}, \quad (3.1)$$

where $\pi^+ = \frac{1}{\sqrt{2}}(\pi_1 - i\pi_2)$, $\pi^- = \frac{1}{\sqrt{2}}(\pi_1 + i\pi_2)$, $\pi^0 = \pi_3$, and $\pi_i = \text{Tr}(\tau_i \pi)$.

To reproduce the chiral-symmetry-breaking pattern, we introduce

$$U = e^{(i\frac{2\pi}{F_0})}, \quad (3.2)$$

where F_0 is the pion decay constant, which will be explained latter. U expands as

$$U = \mathbb{1} + i\frac{2\pi}{F_0} - \frac{(2\pi)^2}{2F_0^2} + \dots \quad (3.3)$$

Under a chiral transformation, U , $\partial_\mu U$, U^\dagger , and $\partial_\mu U^\dagger$ transform as

$$U \rightarrow g_L U g_R^\dagger, \quad (3.4)$$

$$\partial_\mu U \rightarrow \partial_\mu (g_L U g_R^\dagger) = g_L \partial_\mu U g_R^\dagger, \quad (3.5)$$

$$U^\dagger \rightarrow g_R U^\dagger g_L^\dagger, \quad (3.6)$$

$$\partial_\mu U^\dagger \rightarrow \partial_\mu (g_R U^\dagger g_L^\dagger) = g_R \partial_\mu U^\dagger g_L^\dagger. \quad (3.7)$$

Therefore, at the lowest order in the derivatives, the general effective Lagrangian that respects chiral symmetry reads

$$\mathcal{L}_2^{\text{ChPT}} = \frac{F_0^2}{4} \text{Tr}(\partial_\mu U \partial^\mu U^\dagger). \quad (3.8)$$

The covariant derivative of U is

$$\begin{aligned} D_\mu U &= \partial_\mu U - i\mathcal{L}_\mu U + iU\mathcal{R}_\mu \\ &= \partial_\mu U - i\mathcal{L}_\mu^a t^a U + iU\mathcal{R}_\mu^a t^a, \end{aligned} \quad (3.9)$$

where \mathcal{L} and \mathcal{R} are the external fields.

The covariant version of Eq. (3.8) reads

$$\mathcal{L}_2^{\text{ChPT}} = \frac{F_0^2}{4} \text{Tr}(D_\mu U D^\mu U^\dagger). \quad (3.10)$$

From Eq. (3.10), we obtain the corresponding left and right currents as

$$J_{La}^\mu = \frac{\partial \mathcal{L}_2^{\text{ChPT}}}{\partial \mathcal{L}_\mu^a} = -i\frac{F_0^2}{2} \text{Tr}(\tau^a U \partial^\mu U^\dagger), \quad (3.11)$$

$$J_{Ra}^\mu = \frac{\partial \mathcal{L}_2^{\text{ChPT}}}{\partial \mathcal{R}_\mu^a} = i\frac{F_0^2}{2} \text{Tr}(\tau^a \partial^\mu U^\dagger U). \quad (3.12)$$

The vector and axial-vector currents are the combination of Eqs. (3.11) and (3.12), which are expressed as

$$J_{Va}^\mu = \frac{J_{La}^\mu + J_{Ra}^\mu}{2} = -i\frac{F_0^2}{4} \text{Tr}(\tau^a [U, \partial^\mu U^\dagger]), \quad (3.13)$$

$$J_{Aa}^\mu = \frac{-J_{La}^\mu + J_{Ra}^\mu}{2} = i\frac{F_0^2}{4} \text{Tr}(\tau^a \{U, \partial^\mu U^\dagger\}). \quad (3.14)$$

The lowest order of the axial-vector current is obtained by inserting Eq. (3.3) into (3.14), i.e.,

$$J_{Aa}^\mu = i \frac{F_0^2}{4} \text{Tr}(\tau^a \{ \mathbb{1} + \dots, -i \frac{\partial^\mu \pi^a \tau^a}{F_0} + \dots \}) = F_0 \partial^\mu \pi^a \tau^a + \dots \quad (3.15)$$

Evaluating the axial-vector current between the vacuum and the NG boson state, we get that

$$\langle 0 | J_{Aa}^\mu(x) | \pi_b(p) \rangle = F_0 \partial^\mu e^{-ip \cdot x} \delta_{ab} + \dots = -ip^\mu F_0 \delta_{ab} e^{-ip \cdot x} + \dots \quad (3.16)$$

Comparing (3.16) and (2.30), we identify F_0 as the pion decay constant f_π .

3.1.2 Spontaneously symmetry breaking by the quark masses

As stated in Sec. 2.1, the chiral symmetry is broken when the quarks have finite mass. In this subsection, we introduce the quark masses to the theory and discuss the symmetry-breaking pattern.

Recall that the mass term in the QCD Lagrangian (2.9) could be expressed as

$$\mathcal{L}_{m_q}^{\text{QCD}} = -\bar{\psi}_L \mathcal{M} \psi_R - \bar{\psi}_R \mathcal{M}^\dagger \psi_L, \quad (3.17)$$

where \mathcal{M} is the quark mass matrix. When $N_f = 2$, \mathcal{M} is expressed as

$$\mathcal{M} = \begin{pmatrix} m_u & 0 \\ 0 & m_d \end{pmatrix}. \quad (3.18)$$

Under the chiral transform, $\psi_{L,R}$ transform as $\psi_{L,R} \rightarrow g_{L,R} \psi_{L,R}$. Therefore, \mathcal{L}_{m_q} is chiral invariant only if \mathcal{M} transforms as

$$\mathcal{M} \rightarrow g_L \mathcal{M} g_R^\dagger. \quad (3.19)$$

Thus, at the lowest order of \mathcal{M} , the Lagrangian that contains the quark mass term is expressed as

$$\mathcal{L}_{\text{SB}}^{\text{ChPT}} = F_0^2 \frac{B}{2} \text{Tr}(\mathcal{M} U^\dagger + U \mathcal{M}^\dagger), \quad (3.20)$$

which breaks chiral symmetry spontaneously.

In vacuum, the chiral symmetry is spontaneously broken as

$$SU(N_f)_L \times SU(N_f)_R \rightarrow SU(N_f)_V. \quad (3.21)$$

Inserting Eq. (3.3) into (3.20), we get the mass term of the NG bosons as

$$\mathcal{L}_{\text{SB}}^{\text{ChPT}} = F_0^2 \frac{B}{2} \text{Tr}(\mathcal{M} U^\dagger + U \mathcal{M}^\dagger)$$

Operator	Chiral transformation	Charge conjugation	Parity
U	$g_L U g_R^\dagger$	U^T	U^\dagger
$D_\mu U$	$g_L D_\mu U g_R^\dagger$	$(D_\mu U)^T$	$(D^\mu U)^\dagger$
χ	$g_L \chi g_R^\dagger$	χ^T	χ^\dagger
\mathcal{L}_μ	$g_L \mathcal{L}_\mu g_L^\dagger + i g_L \partial_\mu g_L^\dagger$	$-\mathcal{R}_\mu^T$	\mathcal{R}^μ
\mathcal{R}_μ	$g_R \mathcal{R}_\mu g_R^\dagger + i g_R \partial_\mu g_R^\dagger$	$-\mathcal{L}_\mu^T$	\mathcal{L}^μ
$F_{R\mu\nu}$	$g_R F_{R\mu\nu} g_R^\dagger$	$-F_{L\mu\nu}^T$	$F_L^{\mu\nu}$
$F_{L\mu\nu}$	$g_L F_{L\mu\nu} g_L^\dagger$	$-F_{R\mu\nu}^T$	$F_R^{\mu\nu}$

Table 3.1: Transformation properties of the ChPT operators

$$= -B(m_u + m_d)\pi^+\pi^- - \frac{B}{2}(m_u + m_d)\pi^0\pi^0 + \dots \quad (3.22)$$

By comparing Eq. (3.22) to the kinetic term (3.10) we obtain that

$$m_\pi^2 = 2B\hat{m}, \quad (3.23)$$

where m_π is the pion mass and $\hat{m} = m_u = m_d$.

For convenience we introduce

$$\chi = 2B(s + ip), \quad (3.24)$$

where s and p are the scalar and pseudoscalar external fields, respectively. Excluding the pseudoscalar external fields, χ is determined as

$$\chi = 2B \begin{pmatrix} m_u & 0 \\ 0 & m_d \end{pmatrix} = 2B \begin{pmatrix} \hat{m} & 0 \\ 0 & \hat{m} \end{pmatrix} = m_\pi^2 \begin{pmatrix} 1 & 0 \\ 0 & 1 \end{pmatrix}, \quad (3.25)$$

in vacuum.

3.1.3 General Lagrangian

From the previous subsections, 3.1.1 and 3.1.2, we observe that ChPT has two kind of expansions: (i) in the small momenta and (ii) in the quark masses m_q around the chiral limit. The independent operators of chiral perturbation theory are summarized in Table 3.1.

From Table 3.1, we can construct the general Lagrangian that is invariant under chiral transformation, charge conjugation, and parity. The most general Lagrangian for $\mathcal{O}(p^2)$ is

$$\mathcal{L}_2^{\text{ChPT}} = \frac{f_\pi^2}{4} \text{Tr}(D_\mu U D^\mu U^\dagger) + \frac{f_\pi^2}{4} \text{Tr}(\chi U^\dagger + \chi^\dagger U), \quad (3.26)$$

where f_π is the pion decay constant.

For $\mathcal{O}(p^4)$, the general operators are

$$P_0 = \text{Tr}(D_\mu U D_\nu U^\dagger D^\mu U D^\nu U^\dagger), \quad (3.27)$$

$$P_1 = (\text{Tr}(D_\mu U^\dagger D^\mu U))^2, \quad (3.28)$$

$$P_2 = \text{Tr}(D_\mu U^\dagger D_\nu U) \text{Tr}(D^\mu U^\dagger D^\nu U), \quad (3.29)$$

$$P_3 = \text{Tr}(D_\mu U^\dagger D^\mu U D_\nu U^\dagger D^\nu U), \quad (3.30)$$

$$P_4 = \text{Tr}(D_\mu U^\dagger D^\mu U) \text{Tr}(\chi^\dagger U + U^\dagger \chi), \quad (3.31)$$

$$P_5 = \text{Tr}(D_\mu U^\dagger D^\mu U (\chi^\dagger U + U^\dagger \chi)), \quad (3.32)$$

$$P_6 = (\text{Tr}(\chi^\dagger U + \chi U^\dagger))^2, \quad (3.33)$$

$$P_7 = (\text{Tr}(\chi^\dagger U - \chi U^\dagger))^2, \quad (3.34)$$

$$P_8 = \text{Tr}(\chi^\dagger U \chi^\dagger U + \chi U^\dagger \chi U^\dagger), \quad (3.35)$$

$$P_9 = -i \text{Tr}(\mathcal{L}_{\mu\nu} D^\mu U D^\nu U^\dagger), \quad (3.36)$$

$$P_{10} = \text{Tr}(U^\dagger \mathcal{L}_{\mu\nu} U \mathcal{R}^{\mu\nu}), \quad (3.37)$$

$$Q_1 = \text{Tr}(\mathcal{L}_{\mu\nu} \mathcal{L}^{\mu\nu} + \mathcal{R}_{\mu\nu} \mathcal{R}^{\mu\nu}), \quad (3.38)$$

$$Q_2 = \text{Tr}(\chi^\dagger \chi). \quad (3.39)$$

The previous $\mathcal{O}(p^4)$ operators are dependent. For the $N_f = 2$ case, we have the following relations

$$P_1 = -P_0 + P_3, \quad (3.40)$$

$$P_2 = P_0 + P_3, \quad (3.41)$$

$$P_5 = \frac{1}{2} P_4. \quad (3.42)$$

Therefore, limiting the number of flavors to $N_f = 2$ and excluding the external source fields, the Lagrangian of ChPT up to $\mathcal{O}(p^4)$ is written as

$$\begin{aligned} \mathcal{L}_{\mathcal{O}(p^2)+\mathcal{O}(p^4)}^{\text{ChPT}} &= \frac{f_\pi^2}{4} \text{Tr}(D_\mu U D^\mu U^\dagger) \\ &+ l_1 \text{Tr}(D_\mu U D_\nu U^\dagger D^\mu U D^\nu U^\dagger) \\ &+ l_2 \text{Tr}(D_\mu U^\dagger D^\mu U D_\nu U^\dagger D^\nu U). \end{aligned} \quad (3.43)$$

The full Lagrangian up to $\mathcal{O}(p^4)$ is given in Refs. ^[35;36;42]. A review article for the ChPT Lagrangian up to $\mathcal{O}(p^6)$ is given in Ref. ^[43].

The intrinsic parity of the Lagrangian shown in (3.43) is even. In QCD, there are some processes that break parity, leading to a Lagrangian with an odd intrinsic parity part, i.e., the Wess-Zumino-Witten (WZW) term, given in Refs. ^[44-46]. Following Ref. ^[47], the WZW term is expressed as

$$\Gamma_{\text{WZW}} = C \int_{M^5} \text{tr}(\alpha^5) - 5Ci \int_{M^4} \text{tr}[\mathcal{L}\alpha^3 + \mathcal{R}\beta^3]$$

$$\begin{aligned}
& - 5C \int_{M^4} \text{tr} [(d\mathcal{L}\mathcal{L} + \mathcal{L}d\mathcal{L})\alpha + (d\mathcal{R}\mathcal{R} + \mathcal{R}d\mathcal{R})\beta] \\
& - 5Ci \int_{M^4} \text{tr} [d\mathcal{L}dURU^{-1} - d\mathcal{R}dU^{-1}\mathcal{L}U] \\
& + 5Ci \int_{M^4} \text{tr} [\mathcal{R}U^{-1}\mathcal{L}U\beta^2 - \mathcal{L}U\mathcal{R}U^{-1}\alpha^2] \\
& + \frac{5}{2}Ci \int_{M^4} \text{tr} [(\mathcal{L}\alpha)^2 - (\mathcal{R}\beta)^2] + 5Ci \int_{M^4} \text{tr} [\mathcal{L}^3\alpha + \mathcal{R}^3\beta] \\
& + 5C \int_{M^4} \text{tr} [(d\mathcal{R}\mathcal{R} + \mathcal{R}d\mathcal{R})U^{-1}\mathcal{L}U - (d\mathcal{L}\mathcal{L} + \mathcal{L}d\mathcal{L})URU^{-1}] \\
& - 5Ci \int_{M^4} \text{tr} \left[\mathcal{R}^3U^{-1}\mathcal{L}U - \mathcal{L}^3URU^{-1} + \frac{1}{2}(URU^{-1}\mathcal{L})^2 \right] \\
& + 5Ci \int_{M^4} \text{tr} [\mathcal{L}URU^{-1}\mathcal{L}\alpha + \mathcal{R}U^{-1}\mathcal{L}U\mathcal{R}\beta] , \tag{3.44}
\end{aligned}$$

where

$$\begin{aligned}
C &= \frac{N_c}{240\pi^2}, \quad \mathcal{L} \equiv \mathcal{L}_\mu dx^\mu, \quad \mathcal{R} \equiv \mathcal{R}_\mu dx^\mu, \\
\alpha &\equiv \frac{1}{i} (\partial_\mu U) U^{-1} dx^\mu, \quad \beta \equiv U^{-1} \alpha U. \tag{3.45}
\end{aligned}$$

3.2 Hidden local symmetry

In addition to the pion, the vector meson degrees of freedom are also included in the theory to compare with low energy experiment^[48]. In this section, we first discuss HLS and then briefly review the procedure of how to construct the effective Lagrangian within the framework of HLS. Finally, we show that ChPT and HLS have close connections, i.e., if we integrate out the vector meson contribution, we get the corresponding ChPT Lagrangian.

3.2.1 $G_{\text{global}} \times H_{\text{local}}$ symmetry

In this subsection, we briefly review HLS, following^[47;49-51].

Instead of U , the basic quantities needed to reproduce the $G_{\text{global}} \times H_{\text{local}}$ symmetry are ξ_L and ξ_R , where

$$U = \xi_L^\dagger \xi_R. \tag{3.46}$$

Under the $G_{\text{global}} \times H_{\text{local}}$ symmetry, $\xi_{L,R}$ transform as

$$\xi_{L,R}(x) \rightarrow h(x) \xi_{L,R}(x) g_{L,R}^\dagger, \tag{3.47}$$

where

$$h(x) \in H_{\text{local}}, \quad g_{L,R} \in G_{\text{global}}. \quad (3.48)$$

Generally, $\xi_{L,R}$ are parameterized as

$$\xi_{L,R} = e^{i\mathcal{P}/f_{\mathcal{P}}} e^{\mp i\pi/f_{\pi}}, \quad (3.49)$$

where π represents the NG bosons of the G chiral symmetry, \mathcal{P} the NG bosons of the H hidden gauge, and f_{π} and $f_{\mathcal{P}}$ are the relevant decay constants. In the unitary gauge, i.e., $\mathcal{P} \equiv 0$, $\xi_{L,R}$ are written as

$$\xi_L^{\dagger} = \xi_R = \xi = e^{i\pi/f_{\pi}}. \quad (3.50)$$

The covariant derivatives of $\xi_{L,R}$ are

$$D_{\mu}\xi_L = \partial_{\mu}\xi_L - iV_{\mu}\xi_L + i\xi_L\mathcal{L}_{\mu}, \quad (3.51)$$

$$D_{\mu}\xi_R = \partial_{\mu}\xi_R - iV_{\mu}\xi_R + i\xi_R\mathcal{R}_{\mu}, \quad (3.52)$$

where V_{μ} is the NG boson for the H hidden gauge, whereas \mathcal{L} and \mathcal{R} are external fields.

For the $N_f = 2$ case, V_{μ} is expressed as

$$V_{\mu} = \frac{g}{2} \begin{pmatrix} \omega_{\mu} + \rho_{\mu}^0 & \sqrt{2}\rho_{\mu}^+ \\ \sqrt{2}\rho_{\mu}^- & \omega_{\mu} - \rho_{\mu}^0 \end{pmatrix}. \quad (3.53)$$

Instead of $\xi_{L,R}$, it is convenient to define the Maurer-Cartan 1-forms as

$$\begin{aligned} \hat{\alpha}_{\perp\mu} &= (D_{\mu}\xi_R\xi_R^{\dagger} - D_{\mu}\xi_L\xi_L^{\dagger})/(2i), \\ \hat{\alpha}_{\parallel\mu} &= (D_{\mu}\xi_R\xi_R^{\dagger} + D_{\mu}\xi_L\xi_L^{\dagger})/(2i). \end{aligned} \quad (3.54)$$

In HLS, the adjoint representation of χ is expressed as

$$\hat{\chi} = \xi_L\chi\xi_R^{\dagger}. \quad (3.55)$$

The HLS gauge boson and external field are defined as

$$\begin{aligned} V_{\mu\nu} &= \partial_{\mu}V_{\nu} - \partial_{\nu}V_{\mu} - i[V_{\mu}, V_{\nu}], \\ \hat{\mathcal{V}}_{\mu\nu} &= \frac{1}{2}(\xi_R\mathcal{R}_{\mu\nu}\xi_R^{\dagger} + \xi_L\mathcal{L}_{\mu\nu}\xi_L^{\dagger}), \\ \hat{\mathcal{A}}_{\mu\nu} &= \frac{1}{2}(\xi_R\mathcal{R}_{\mu\nu}\xi_R^{\dagger} - \xi_L\mathcal{L}_{\mu\nu}\xi_L^{\dagger}). \end{aligned} \quad (3.56)$$

The operators for HLS under charge conjugation, parity, and gauge transform are summarized in Table 3.2.

Operator	$G \times H$	Charge conjugation	Parity
$\hat{\alpha}_{\perp\mu}$	$h(x)\hat{\alpha}_{\perp\mu}h(x)^\dagger$	$\hat{\alpha}_{\perp\mu}^T$	$-\hat{\alpha}_{\perp}^\mu$
$\hat{\alpha}_{\parallel\mu}$	$h(x)\hat{\alpha}_{\parallel\mu}h(x)^\dagger$	$-\hat{\alpha}_{\parallel\mu}^T$	$\hat{\alpha}_{\parallel}^\mu$
$\hat{\chi}$	$h(x)\hat{\chi}h(x)^\dagger$	$\hat{\chi}^T$	$\hat{\chi}^\dagger$
$V_{\mu\nu}$	$h(x)V_{\mu\nu}h(x)^\dagger$	$-V_{\mu\nu}^T$	$V^{\mu\nu}$
$\hat{V}_{\mu\nu}$	$h(x)\hat{V}_{\mu\nu}h(x)^\dagger$	$-\hat{V}_{\mu\nu}^T$	$\hat{V}^{\mu\nu}$
$\hat{A}_{\mu\nu}$	$h(x)\hat{A}_{\mu\nu}h(x)^\dagger$	$\hat{A}_{\mu\nu}^T$	$-\hat{A}^{\mu\nu}$

Table 3.2: Transformation properties of HLS operators

3.2.2 General Lagrangian

Using the operators listed in Table 3.2, we construct the lowest order HLS Lagrangian up to $\mathcal{O}(p^2)$ as

$$\begin{aligned} \mathcal{L}_2^{\text{HLS}} &= f_\pi^2 \text{Tr}(\hat{\alpha}_{\perp\mu}\hat{\alpha}_{\perp}^\mu) + a_{\text{hls}}f_\pi^2 \text{Tr}(\hat{\alpha}_{\parallel\mu}\hat{\alpha}_{\parallel}^\mu) \\ &\quad - \frac{1}{2g^2} \text{Tr}(V_{\mu\nu}V^{\mu\nu}) + \frac{1}{4}f_\chi^2 \text{Tr}(\hat{\chi} + \hat{\chi}^\dagger), \end{aligned} \quad (3.57)$$

where a_{hls} is a real dimensionless parameter, g the gauge coupling constant of the HLS, and $f_\chi = f_\pi$ at tree level.

For even intrinsic parity parts, the order $\mathcal{O}(p^4)$ HLS Lagrangian is given in Refs. [47;52]. The odd intrinsic parity terms of the Lagrangian $\mathcal{L}_{\text{anom}}$ are related to the $U(2)_L \times U(2)_R$ chiral anomaly, which is given as [47;53;54]

$$\int d^4x \mathcal{L}_{\text{anom}} = \Gamma_{\text{WZW}} + \frac{N_c}{16\pi^2} \int_{M^4} \sum_{i=1}^3 c_i \mathcal{L}_i, \quad (3.58)$$

where Γ_{WZW} is given in Eq. (3.44), M^4 represents the four-dimensional Minkowski space, and

$$\begin{aligned} \mathcal{L}_1 &= i\epsilon^{\mu\nu\sigma\rho} \text{Tr}(\alpha_{L\mu}\alpha_{L\nu}\alpha_{L\sigma}\alpha_{R\rho} - \alpha_{R\mu}\alpha_{R\nu}\alpha_{R\sigma}\alpha_{L\rho}), \\ \mathcal{L}_2 &= i\epsilon^{\mu\nu\sigma\rho} \text{Tr}(\alpha_{L\mu}\alpha_{R\nu}\alpha_{L\sigma}\alpha_{R\rho}), \\ \mathcal{L}_3 &= \epsilon^{\mu\nu\sigma\rho} \text{Tr}[F_{V\mu\nu}(\alpha_{L\sigma}\alpha_{R\rho} - \alpha_{R\sigma}\alpha_{L\rho})], \\ \mathcal{L}_4 &= \epsilon^{\mu\nu\sigma\rho} \text{Tr}\left[(\hat{F}_{\mathcal{L}\mu\nu} + \hat{F}_{\mathcal{R}\mu\nu})(\alpha_{L\sigma}\alpha_{R\rho} - \alpha_{R\sigma}\alpha_{L\rho})\right], \end{aligned} \quad (3.59)$$

in terms of the 1-form and 2-form notation. Here, $\alpha_L = \hat{\alpha}_{\parallel} - \hat{\alpha}_{\perp}$, $\alpha_R = \hat{\alpha}_{\parallel} + \hat{\alpha}_{\perp}$, $F_V = dV - iV^2$, $\hat{F}_{\mathcal{L},\mathcal{R}} = \xi_{L,R}F_{\mathcal{L},\mathcal{R}}\xi_{L,R}^\dagger$, $F_{\mathcal{L}} = d\mathcal{L} - i\mathcal{L}^2$, and $F_{\mathcal{R}} = d\mathcal{R} - i\mathcal{R}^2$.

3.2.3 Relations between HLS and ChPT

Previously, we discussed the general formula of the HLS and ChPT Lagrangians. These two types of Lagrangians are closely related if we integrate out the vector meson contribution. This will be shown in this subsection.

Note that $\hat{\alpha}_{\perp\mu}$ and $V_{\mu\nu}$ can be rewritten as

$$\hat{\alpha}_{\perp\mu} = -\frac{i}{2}\xi_L D_\mu U \xi_R^\dagger, \quad (3.60)$$

and

$$\begin{aligned} V_{\mu\nu} &= \hat{V}_{\mu\nu} + i[\hat{\alpha}_{\perp\mu}, \hat{\alpha}_{\parallel\nu}] + \frac{1}{m_\rho^2} \mathcal{O}(p^4) \\ &= \xi_L \left(\frac{1}{2} U \mathcal{R}_{\mu\nu} + \frac{1}{2} \mathcal{L}_{\mu\nu} + \frac{i}{4} D_\mu U D_\nu U^\dagger - \frac{i}{4} D_\nu U D_\mu U^\dagger \right) \xi_L^\dagger \\ &\quad + \frac{1}{m_\rho^2} \mathcal{O}(p^4). \end{aligned} \quad (3.61)$$

Insert Eqs. (3.60) and (3.61) into Eq. (3.57). For the $N_f = 2$ case, we get that

$$f_\pi^2 \text{Tr}(\hat{\alpha}_{\perp\mu} \hat{\alpha}_{\perp}^\mu) = \frac{f_\pi^2}{4} \text{Tr}(D_\mu U^\dagger D^\mu U), \quad (3.62)$$

$$a_{\text{hls}} f_\pi^2 \text{Tr}(\hat{\alpha}_{\parallel\mu} \hat{\alpha}_{\parallel}^\mu) = \mathcal{O}(p^6), \quad (3.63)$$

$$\begin{aligned} -\frac{1}{2g^2} \text{Tr}(V_{\mu\nu} V^{\mu\nu}) &= \frac{1}{16g^2} \text{Tr}(D_\mu U D_\nu U^\dagger D^\mu U D^\nu U^\dagger) \\ &\quad - \frac{1}{16g^2} \text{Tr}(D_\mu U^\dagger D^\mu U D_\nu U^\dagger D^\nu U) \\ &\quad - i \frac{1}{4g^2} \text{Tr}(\mathcal{L}_{\mu\nu} D^\mu U D^\nu U^\dagger + \mathcal{R}_{\mu\nu} D^\mu U^\dagger D^\nu U) \\ &\quad - \frac{1}{4g^2} \text{Tr}(\mathcal{L}_{\mu\nu} U \mathcal{R}^{\mu\nu} U^\dagger) \\ &\quad - \frac{1}{8g^2} \text{Tr}(\mathcal{L}_{\mu\nu} \mathcal{L}^{\mu\nu} + \mathcal{R}_{\mu\nu} \mathcal{R}^{\mu\nu}), \end{aligned} \quad (3.64)$$

$$\frac{1}{4} f_\chi^2 \text{Tr}(\hat{\chi} + \hat{\chi}^\dagger) = \frac{f_\pi^2}{4} \text{Tr}(\chi U^\dagger + \chi^\dagger U). \quad (3.65)$$

By comparing the Lagrangians of HLS ($\mathcal{O}(p^2)$) and ChPT ($\mathcal{O}(p^4)$), we conclude that they are consistent with each other when we integrate out the vector meson contributions.

Chapter 4

Skyrme model

In this chapter, we consider the baryon as the soliton solution of mesonic models.

The original idea was proposed by Skyrme in 1962, and it has since been extended widely in several studies. The original idea was to identify the topological solution of the nonlinear sigma model with the baryon. In the beginning the Lagrangian is a particular choice from ChPT up to $\mathcal{O}(p^4)$. To construct a realistic way to reproduce the meson and baryon properties, the ρ and ω mesons are introduced within the framework of HLS to build the baryon state.

However, the appearance of the ω meson generates a strong repulsive force, which raises the lightest baryon mass by approximately 50%. Introducing a dilaton-type scalar meson shows that the attractive force made from the scalar meson drops the baryon mass.

In this chapter, we review baryon properties in the skyrmion model. In Sec. 4.3, based on our study in Ref. ^[55], we discuss the baryon properties with scalar mesons.

4.1 Skyrme model with the pion

The original skyrmion model only contains the pion degrees of freedom, constructed within the framework of ChPT. We start the discussion from ChPT and then consider the baryon properties for a single skyrmion.

4.1.1 The model

In 1962, Skyrme proposed a way to construct the baryon as the soliton of the pion^[12].

The action of the model is written as

$$\Gamma = \int d^4x \mathcal{L} + \Gamma_{\text{WZW}}, \quad (4.1)$$

where $\Gamma_{\text{WZW}} \equiv \int d^4x \mathcal{L}_{\text{WZW}}$ is the WZW term (3.44), and the Lagrangian \mathcal{L} is a particular choice of the ChPT Lagrangian (3.43), as

$$\mathcal{L} = \frac{f_\pi^2}{16} \text{Tr}(D_\mu U^\dagger D^\mu U) + \frac{1}{32g_{\text{sky}}^2} \text{Tr}([U^\dagger D_\mu U, U^\dagger D_\nu U]^2). \quad (4.2)$$

Here g_{sky} is a dimensionless coupling constant.

The baryon number current of the model is obtained by a functional derivative of the WZW term with $\mathcal{V}_{B\mu}$, i.e.,

$$j_B^\mu = \frac{\partial \mathcal{L}_{\text{WZW}}}{\partial (\mathcal{V}_{B\mu})} \Big|_{\mathcal{V}_{B\mu} \rightarrow 0}, \quad (4.3)$$

where $\mathcal{V}_{B\mu}$ is the external gauge field of the $U(1)_V$ baryon number.

To perform the calculation, Skyrme proposed the hedgehog ansatz to correlate the spin and isospin as

$$U = e^{i\boldsymbol{\tau} \cdot \hat{\mathbf{r}} F(r)}. \quad (4.4)$$

The demonstration of the hedgehog ansatz is shown in Fig. 4.1.

The baryon number N_B is obtained as

$$\begin{aligned} N_B &= \int d^3x j_B^0 \\ &= \int dr \left(-4\pi r^2 \frac{F' \sin^2(F)}{2\pi^2 r^2} \right) \\ &= \frac{\sin(F(r)) \cos(F(r)) - F(r)}{\pi} \Big|_{F(0)=n\pi}^{F(\infty)=0} \\ &= n, \end{aligned} \quad (4.5)$$

where the boundary conditions $F(\infty) = 0$ and $F(0) = n\pi$ are imposed. In the following discussions, we consider the single baryon state with $n = 1$.

Inserting the ansatz equation (4.4) in the Lagrangian (4.2) and after performing the scale transformation $r \rightarrow \frac{a_{\text{sky}}}{g_{\text{sky}} f_\pi} r$, we get the static mass for the skyrmion as

$$M_{\text{sol}} = \int dr \frac{\pi f_\pi \left(r^2 (F'^2 (r^2 a_{\text{sky}}^2 + 8 \sin^2 F) + 2a_{\text{sky}}^2 \sin^2 F) + 4 \sin^4 F \right)}{2r^2 a_{\text{sky}} g_{\text{sky}}}. \quad (4.6)$$

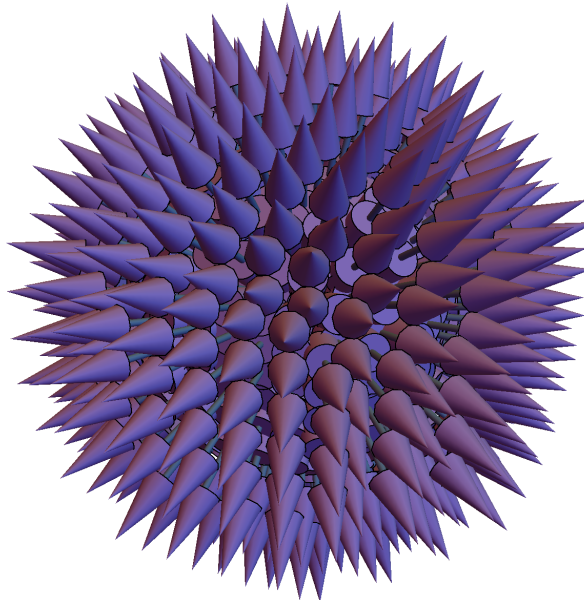


Figure 4.1: Hedgehog ansatz

The equation of motion for $F(r)$ is

$$F'' = \frac{r^2 (a_{\text{sky}}^2 (\sin(2F) - 2rF') - 4F'^2 \sin(2F)) + 8 \sin^3(F) \cos(F)}{r^4 a_{\text{sky}}^2 + 8r^2 \sin^2(F)}. \quad (4.7)$$

The equation of motion shown in (4.7) is very complicated, but we can get the solution of $F(r)$ numerically. It is shown in Fig. 4.2.

The baryon mass (4.6) depends on the parameter g_{sky} . Therefore we adjust the skyrmion mass by controlling the parameter g_{sky} .

4.1.2 Quantize the skyrmion

The original Skyrme model only contains the baryon number N_B . However, the physical baryon state preserves spin and isospin. To introduce the spin and isospin states, Adkins-Nappi-Witten proposed a systematic way to quantize the skyrmion^[56]. We review the properties of the quantized skyrmion by following Ref.^[56].

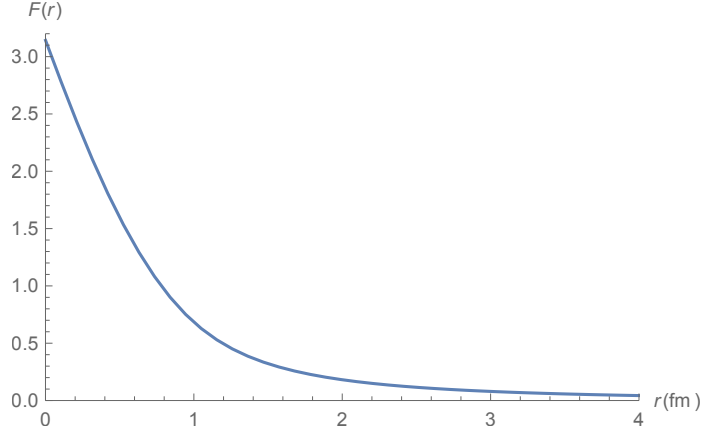


Figure 4.2: Profile function for $F(r)$

The starting point is to introduce the time dependent rotation of U as

$$U = A(t)\tilde{U}A(t)^\dagger = \tilde{U}(R(t)^{-1}r), \quad (4.8)$$

where $A(t)$ and $R(t)$ are $SU(2)$ and $SO(3)$ matrices, respectively. The isospin rotation T and spin rotation Ω are

$$A^{-1}\dot{A} = \frac{i}{2}T_a\tau_a, \quad (R^{-1}\dot{R})_{ij} = \epsilon_{ijk}\Omega_k. \quad (4.9)$$

For the present purpose, and because spin and isospin are related to each other, Ω and T are dependent. For convenience, here we choose to consider only the T rotation for convenience.

Inserting (4.8) into (4.2) we get that

$$\int d^3r \mathcal{L} = -M_{\text{sol}} + \frac{1}{2}\Lambda (T_1^2 + T_2^2 + T_3^2), \quad (4.10)$$

where

$$\Lambda = \int dr \frac{2\pi a_{\text{sky}} \sin^2(F) (a_{\text{sky}}^2 r^2 + 4r^2 F'^2 - 2 \cos(2F) + 2)}{3g_{\text{sky}}^3 f_\pi}. \quad (4.11)$$

The isospin and spin angular momentum are obtained as

$$I_i = J_i = \frac{\partial \mathcal{L}}{\partial T_i} = \Lambda_i T_i. \quad (4.12)$$

Thus, the Hamiltonian up to $\mathcal{O}(N_c^{-1})$ can be expressed as

$$\mathcal{H} = M_{\text{sol}} + \frac{I_1^2 + I_2^2 + I_3^2}{2\Lambda}. \quad (4.13)$$

The isospin and spin operators are expressed as

$$I_k = \frac{i}{2} \left(a_0 \frac{\partial}{\partial a_k} - a_k \frac{\partial}{\partial a_0} - \varepsilon_{klm} a_l \frac{\partial}{\partial a_m} \right), \quad (4.14)$$

$$J_k = \frac{i}{2} \left(a_k \frac{\partial}{\partial a_0} - a_0 \frac{\partial}{\partial a_k} - \varepsilon_{klm} a_l \frac{\partial}{\partial a_m} \right), \quad (4.15)$$

where $k \in (1, 2, 3)$, $a_0 = \frac{1}{2} \text{Tr}(A(t))$, and $a_k = \frac{1}{2} \text{Tr}(A(t)\tau_k)$.

The normalized wave functions for some physical baryon states are given by

$$|p \uparrow\rangle = \frac{1}{\pi} (a_1 + ia_2), \quad |p \downarrow\rangle = -\frac{i}{\pi} (a_0 - ia_3), \quad (4.16)$$

$$|n \uparrow\rangle = \frac{i}{\pi} (a_0 + ia_3), \quad |n \downarrow\rangle = -\frac{1}{\pi} (a_1 - ia_2), \quad (4.17)$$

$$|\Delta^{++}, s_z = \frac{3}{2}\rangle = \frac{\sqrt{2}}{\pi} (a_1 + ia_2)^3, \quad (4.18)$$

$$|\Delta^+, s_z = \frac{1}{2}\rangle = -\frac{\sqrt{2}}{\pi} (a_1 + ia_2)(1 - 3(a_0^2 + a_3^2)). \quad (4.19)$$

The mass of the skyrmion for a given state is obtained as

$$\langle X | \mathcal{H} | X \rangle = M_{\text{sol}} + \frac{1}{2\Lambda} I(I+1), \quad (4.20)$$

where X represent the physical baryon state and I the corresponding isospin quantum number.

For the nucleon and delta, the isospins are $I = \frac{1}{2}$ and $I = \frac{3}{2}$, respectively. Thus, the masses of the nucleon and delta are obtained as

$$m_N = M_{\text{sol}} + \frac{1}{2\Lambda} \frac{3}{4}, \quad (4.21)$$

$$m_\Delta = M_{\text{sol}} + \frac{1}{2\Lambda} \frac{15}{4}. \quad (4.22)$$

Treating the masses of the nucleon and delta as inputs, we determine the parameter set: $f_\pi = 127\text{MeV}$, $a_{\text{sky}} = 1$, and $g_{\text{sky}} = 5.34$. The inputs and predictions of the quantized skyrmion are summarized in Table 4.1. From Table 4.1, we observe that the prediction of the baryon properties are consistent with experiment results within $1/N_c \sim 30\%$.

4.2 Skyrme model with π , ρ , and ω mesons

In the last section, we briefly reviewed the original skyrmion, which only contains pion fields. In addition to the pion, the vector meson are also introduced to

Quantity	Prediction	Experiment
m_N	input	939 MeV
m_Δ	input	1232 MeV
f_π	127 MeV	92.4 MeV
$\langle r^2 \rangle_{I=0}^{1/2}$	0.59 fm	0.72 fm
$\langle r^2 \rangle_{M,I=0}^{1/2}$	0.92 fm	0.81 fm

Table 4.1: Inputs and predictions of the quantized skyrmion

construct the skyrmion model^[14–17;57]. As shown in subsection 3.2.3, vector meson exchange plays a role similar to that of the $\mathcal{O}(p^4)$ Lagrangian in the skyrmion model (4.2). The benefit of including the vector meson is that, instead of the model parameter g_{sky} , we can determine the parameters from the low energy constant of HLS.

4.2.1 The model

Following Refs.^[14–17], we start constructing the Skyrme model in the framework of HLS.

The action of the model is written as

$$\Gamma = \int d^4x \mathcal{L} + \int d^4x \mathcal{L}_{\text{anom}}, \quad (4.23)$$

where $\int d^4x \mathcal{L}_{\text{anom}}$ is the anomaly term given in Eq. (3.58). Here, the Lagrangian \mathcal{L} is the HLS Lagrangian (3.57), which reads

$$\begin{aligned} \mathcal{L} &= f_\pi^2 \text{Tr}(\hat{\alpha}_{\perp\mu} \hat{\alpha}_{\perp}^\mu) + a_{\text{hls}} f_\pi^2 \text{Tr}(\hat{\alpha}_{\parallel\mu} \hat{\alpha}_{\parallel}^\mu) \\ &\quad - \frac{1}{2g^2} \text{Tr}(V_{\mu\nu} V^{\mu\nu}) - (V_{SB} - \bar{V}_{SB}), \end{aligned} \quad (4.24)$$

where

$$\begin{aligned} V_{SB} &= -\frac{1}{4} f_\pi^2 \text{Tr}(\hat{\chi} + \hat{\chi}^\dagger) \\ &= -\frac{1}{4} f_\pi^2 m_\pi^2 \text{Tr}(U + U^\dagger). \end{aligned} \quad (4.25)$$

Here, \bar{V}_{SB} is the vacuum state of V_{SB} , which is expressed as

$$\bar{V}_{SB} = -\frac{1}{4} f_\pi^2 m_\pi^2 \text{Tr}(\mathbb{1} + \mathbb{1}). \quad (4.26)$$

To study the properties of the skyrmion obtained from the Lagrangian (4.24), we take the standard parameterizations for soliton configurations. Following Refs.^[12;58], we take the ansatz for the π , ρ , and ω fields:

$$U = e^{i\boldsymbol{\tau}\cdot\hat{\mathbf{r}}F(r)}, \quad (4.27a)$$

$$\boldsymbol{\rho} = \frac{G(r)}{gr}(\hat{\mathbf{r}} \times \boldsymbol{\tau}), \quad (4.27b)$$

$$\omega_\mu = W(r)\delta_{\mu 0}. \quad (4.27c)$$

For the solutions with the baryon number $N_B = n$, the wave functions $F(r)$, $G(r)$, and $W(r)$ satisfy the following boundary conditions:

$$\begin{aligned} F(0) &= n\pi, & F(\infty) &= 0, \\ G(0) &= -1 + (-1)^n, & G(\infty) &= 0, \\ W'(0) &= 0, & W(\infty) &= 0. \end{aligned} \quad (4.28)$$

In this study, we consider only the $N_B = 1$ case, with $n = 1$.

4.2.2 Collective quantization of the skyrmion

By rotating the $K = I + J$ spin of the skyrmion, we get the corresponding masses of m_N and m_Δ .

Following Ref.^[58], we introduce the collective quantization as

$$U(r, t) = A(t)U(r)A^\dagger(t), \quad (4.29)$$

$$\vec{\tau} \cdot \vec{\rho}^0(r, t) = \frac{1}{g}A(t)\vec{\tau} \cdot [\vec{T}\xi_1(r) + \hat{r}\vec{T} \cdot \hat{r}\xi_2(r)]A^\dagger(t), \quad (4.30)$$

$$\vec{\omega}(r, t) = \frac{1}{2} \frac{\xi_3(r)}{r} \vec{T} \times \hat{r}, \quad (4.31)$$

$$\vec{\tau} \cdot \vec{\rho}^i(r, t) = A(t)\vec{\tau} \cdot \vec{\rho}^i A^\dagger(t), \quad (4.32)$$

where

$$A^{-1}\dot{A} = \frac{i}{2}T_a\tau_a. \quad (4.33)$$

Performing a procedure similar to that in Sec. 4.1.2, we quantize the skyrmion. Following Ref.^[58], we summarize the baryon properties of the model in Table 4.2.

From Table 4.2, we observe that the skyrmion mass m_N obtained from the model is approximately 50% heavier than the experimental observation. This implies that only considering the dynamics of the pion, rho, and omega mesons is not enough to reproduce the physical baryon properties.

Quantity	Prediction	Experiment
m_N	1575 MeV	939 MeV
$m_\Delta - m_N$	437 MeV	293 MeV
f_π	input	92.4 MeV
g	5.85 (input)	5.80 ± 0.91
a_{hls}	2 (input)	2.07 ± 0.33
$\langle r^2 \rangle_{E,p}^{1/2}$	0.98 fm	0.86 ± 0.01 fm
$\langle r^2 \rangle_{E,n}^{1/2}$	-0.25 fm	-0.119 ± 0.004 fm
$\langle r^2 \rangle_{M,p}^{1/2}$	0.94 fm	0.86 ± 0.06 fm
$\langle r^2 \rangle_{M,n}^{1/2}$	0.93 fm	0.88 ± 0.07 fm

Table 4.2: Inputs and predictions of the collective quantized skyrmion when $a_{\text{hls}} = 2$

4.3 Skyrme model with light scalar mesons

From the previous section, we observe that the skyrmion mass obtained from the model that contains the pion, rho, and omega mesons is approximately 50% heavier than the mass of the lightest baryon^[17;58]. Later on, it was observed that the attractive effect of the dilaton scalar drops the skyrmion mass by approximately 100 MeV^[20]. In this section, we study the effects of light scalar mesons on the skyrmion following Ref.^[55].

4.3.1 The model

Instead of the dilaton^[20], we study the scalar meson within the framework of the quark model^[27]. In the $N_f = 2$ case, the two-quark state has 4 scalar (σ , \vec{a}_0) and 4 pseudoscalar ($\vec{\pi}$, η) states. The four-quark state has 1 scalar ϕ and 1 pseudoscalar η_0 state. For the present purpose, we only consider σ , $\vec{\pi}$, and ϕ .

We start by constructing a chiral effective model that includes two- and four-quark scalar states. In the $N_f = 2$ case, we write the two-quark field $M_{(2)}$ at the quark level as

$$(M_{(2)})^j_i \sim \bar{q}_{Ri} q_{Lj}. \quad (4.34)$$

Here i, j are the flavor indices with $i, j \in (1, 2)$.

At the hadron level, Eq. (4.34) is rewritten as

$$M_{(2)} = \frac{1}{2} (\sigma + i\vec{\pi} \cdot \vec{\tau}), \quad (4.35)$$

where $\vec{\tau}$ is the Pauli matrices, σ is the isosinglet scalar field and π the isotriplet pseudoscalar fields.

The chiral transformation of the matrix $M_{(2)}$ is

$$M_{(2)} \rightarrow g_L M_{(2)} g_R^\dagger, \quad (4.36)$$

where $g_{L,R} \in \text{SU}(2)_{L,R}$.

At the quark level, the four-quark field is written as

$$\phi \sim \bar{q}_{Li} \bar{q}_{Lj} \epsilon^{ij} q_R^k q_R^l \epsilon_{kl}. \quad (4.37)$$

The two- and four-quark states are separated using the Z_2 symmetry, a remnant of the $U(1)_A$ transformation. Under the Z_2 symmetry, q_L and q_R transforms as

$$q_L \rightarrow -q_L, \quad (4.38)$$

$$q_R \rightarrow q_R, \quad (4.39)$$

respectively. Therefore, the hadron field $M_{(2)}$ and ϕ transform as

$$M_{(2)} \rightarrow -M_{(2)}. \quad (4.40)$$

$$\phi \rightarrow \phi. \quad (4.41)$$

Combining the chiral and Z_2 symmetries, we construct the Lagrangian

$$\begin{aligned} \mathcal{L} = & \text{Tr} \left(\partial_\mu M_{(2)} \partial^\mu M_{(2)}^\dagger \right) + \frac{1}{2} \partial_\mu \phi \partial^\mu \phi \\ & - (V_0 - \bar{V}_0) - (V_{\text{SB}} - \bar{V}_{\text{SB}}), \end{aligned} \quad (4.42)$$

where V_0 represents the potential term of the scalar mesons and V_{SB} is the explicit chiral symmetry breaking term. In vacuum, the potentials V_0 and V_{SB} spontaneously breaks. As a result, they have VEVs of \bar{V}_0 and \bar{V}_{SB} , respectively.

In the present analysis, following Ref. ^[27], we impose some limitations on the potential V_0 and V_{SB} : (i) no derivative interactions appears, (ii) the number of fields included in each vertex is less than or equal to four, and (iii) the number of quarks appearing in each vertex is less than or equal to eight. Thus, the potential take the form

$$\begin{aligned} V_0 = & \lambda \text{Tr} \left(M_{(2)} M_{(2)}^\dagger M_{(2)} M_{(2)}^\dagger \right) - m_2^2 \text{Tr} \left(M_{(2)} M_{(2)}^\dagger \right) + \frac{1}{2} m_4^2 \phi^2 \\ & + \sqrt{2} A \left(\det \left(M_{(2)} \right) + \det \left(M_{(2)}^\dagger \right) \right) \phi, \end{aligned} \quad (4.43)$$

where λ , m_2 , m_4 , and A are model parameters. For the explicit chiral symmetry breaking potential V_{SB} , recall that in the HLS case we have the formula given by Eq. (4.25). For the present purpose, we adopt the potential V_{SB} in the simplest form as

$$V_{\text{SB}} = -\frac{1}{2} f_\pi \text{Tr} \left(\chi M_{(2)}^\dagger + \chi^\dagger M_{(2)} \right), \quad (4.44)$$

where $\chi = 2B\mathcal{M}$, B a constant with dimension one, and \mathcal{M} the quark mass matrix. In the present analysis, we also impose isospin symmetry to simplify the problem. Thus, we have $\mathcal{M} = \text{diag}(\bar{m}, \bar{m})$, where $\bar{m} = (m_u + m_d)/2$. The parameter B is determined from Eq. (3.23), so V_{SB} is expressed as

$$V_{\text{SB}} = -\frac{1}{2}f_\pi m_\pi^2 \text{Tr} \left(M_{(2)}^\dagger + M_{(2)} \right). \quad (4.45)$$

In this thesis, we also include the rho and omega mesons within the framework of HLS^[47;51]. For the present purpose, we take the polar decomposition of $M_{(2)}$ as $M_{(2)} = \frac{1}{2}\xi_L^\dagger \sigma \xi_R$, where ξ_L and ξ_R are given in Eq. (3.49). Here, we consider the unitary gauge of HLS, where ξ_L and ξ_R are expressed by the pion fields based on Eq. (3.50).

Then, the Lagrangian (4.42) is rewritten as

$$\begin{aligned} \mathcal{L} = & \frac{1}{2}\partial_\mu \sigma \partial^\mu \sigma + \sigma^2 \text{Tr} (\hat{\alpha}_{\perp\mu} \hat{\alpha}_{\perp}^\mu) + \frac{1}{2}\partial_\mu \phi \partial^\mu \phi \\ & - (V_0 - \bar{V}_0) - (V_{\text{SB}} - \bar{V}_{\text{SB}}) + \mathcal{L}_V, \end{aligned} \quad (4.46)$$

where $\hat{\alpha}_{\perp\mu}$ is given in Eq. (3.54) and the newly introduced term \mathcal{L}_V represents the Lagrangian for the vector meson component, which will be given explicitly later. The potentials V_0 and V_{SB} are rewritten as

$$\begin{aligned} V_0 &= \frac{1}{8}\lambda\sigma^4 - \frac{1}{2}m_2^2\sigma^2 + \frac{1}{2}m_4^2\phi^2 + \frac{1}{\sqrt{2}}A\sigma^2\phi, \\ V_{\text{SB}} &= -\frac{1}{4}m_\pi^2 f_\pi \sigma \text{Tr} (U + U^\dagger), \end{aligned} \quad (4.47)$$

where U is given in Eq. (3.2).

The potential V_0 and $V = V_0 + V_{\text{SB}}$ are similar to the patterns (ii) and (iii), respectively, and are shown in Fig. 2.1. Therefore, the potential V is broken spontaneously. The stationary conditions of the system are obtained by taking the first derivative of the potential V with respect to σ and ϕ :

$$\frac{\partial V}{\partial \sigma} = \frac{1}{2}\lambda\sigma^3 - m_2^2\sigma + \sqrt{2}A\sigma\phi - m_\pi^2 f_\pi, \quad (4.48)$$

$$\frac{\partial V}{\partial \phi} = m_4^2\phi + \frac{1}{\sqrt{2}}A\sigma^2. \quad (4.49)$$

From Eq. (4.48), we observe that, after a suitable choice of the model parameters λ , m_2 , m_4 , and m_π , σ obtains a VEV σ_{vac} . When A is a nonzero value, ϕ interacts with σ . From Eq. (4.49), we observe that ϕ acquires a VEV ϕ_{vac} .

The physical scalar meson fields are the fluctuations around the VEVs. Then we have the relation that

$$\sigma = f_\pi + \tilde{\sigma}, \quad (4.50)$$

$$\phi = \phi_{\text{vac}} + \tilde{\phi}, \quad (4.51)$$

where $\phi_{\text{vac}} = -\frac{Af_\pi^2}{\sqrt{2}m_4^2}$, which is shown in Eq. (A.4).

The mass matrices for σ and ϕ are obtained by taking the second-order derivative of the corresponding fields, i.e.,

$$\begin{pmatrix} m_\sigma^2 & m_{\sigma\phi}^2 \\ m_{\phi\sigma}^2 & m_\phi^2 \end{pmatrix} = \begin{pmatrix} \lambda f_\pi^2 + m_\pi^2 & \sqrt{2}Af_\pi \\ \sqrt{2}Af_\pi & m_4^2 \end{pmatrix}. \quad (4.52)$$

The two- and four-quark states σ and ϕ are related to the physical states f_{500} and f_{1370} through the rotation

$$\begin{pmatrix} f_{500} \\ f_{1370} \end{pmatrix} = \begin{pmatrix} \cos\theta & -\sin\theta \\ \sin\theta & \cos\theta \end{pmatrix} \begin{pmatrix} \tilde{\sigma} \\ \tilde{\phi} \end{pmatrix}, \quad (4.53)$$

where θ is the mixing angle. Some relations among the parameters and the physical quantities are shown in Appendix A. From Eq. (4.53), one can observe that: (i) when $\cos\theta \rightarrow 0$, the physical state f_{500} is almost a four-quark state and f_{1370} is almost a two-quark state and (ii) when $\cos\theta \rightarrow 1$, f_{500} is dominantly a two-quark state, but f_{1370} is dominantly a four-quark state.

Next, we describe the vector meson components of the Lagrangian. We use the following form:

$$\mathcal{L}_V = \mathcal{L}_{V_0} + \mathcal{L}_{\text{anom}}, \quad (4.54)$$

where \mathcal{L}_{V_0} is the Lagrangian with even intrinsic parity terms, whereas $\mathcal{L}_{\text{anom}}$ is the Lagrangian with odd intrinsic parity terms, given in (3.58).

Explicitly, the even intrinsic parity Lagrangian \mathcal{L}_{V_0} is expressed as

$$\begin{aligned} \mathcal{L}_{V_0} &= a_{\text{hls}}(s_0\sigma^2 + (1-s_0)F^2) \text{Tr}(\hat{\alpha}_{\parallel\mu}\hat{\alpha}_{\parallel}^\mu) \\ &\quad - \frac{1}{2g^2} \text{Tr}(V_{\mu\nu}V^{\mu\nu}), \end{aligned} \quad (4.55)$$

where $\hat{\alpha}_{\parallel}^\mu$ and $V_{\mu\nu}$ are defined as (3.54) and (3.56), respectively. Here s_0 is a real dimensionless parameter, and F is a constant of dimension one.

When we take VEV of σ as $\sigma_{\text{vac}} = f_\pi$, the mass term for the vector meson is expressed as

$$m_V^2 = a_{\text{hls}}g^2(s_0f_\pi^2 + (1-s_0)F^2). \quad (4.56)$$

Equation (4.56) has two parts, the first part, $a_{\text{hls}}g^2s_0f_\pi^2$, represents the vector meson mass obtained by spontaneous chiral symmetry breaking, whereas the second part, $a_{\text{hls}}g^2(1-s_0)F^2$, represents the chiral invariant mass. In this sense, s_0 represents the magnitude of the vector meson mass related to spontaneous chiral

symmetry breaking. In this thesis, we take $F = f_\pi$. Therefore, the vector meson mass is written as

$$m_V^2 = a_{\text{hls}} g^2 f_\pi^2, \quad (4.57)$$

which is consistent with the standard form of the vector meson mass given in HLS^[47:51]. Note that we already have imposed the Z_2 symmetry. Therefore, the term linear in the σ field is excluded in \mathcal{L}_{V_0} . Additionally, s_0 can be both positive and negative in the present analysis.

The low energy constants c_1 , c_2 , and c_3 in the anomaly term (3.58) are usually estimated from the experimental data^[47]. In this section, the focus is on the effect of light scalar mesons on skyrmion properties. Therefore, we choose the set of parameters $c_1 = -c_2 = -2/3$ and $c_3 = 0$, which provides $\omega_\mu B^\mu$ ^[58].

4.3.2 The ansatz

In the Skyrme approach, we need to specify the spin and isospin indices. The ansatz for the pion, rho, and omega mesons is given in Eq. (4.27).

In the present analysis, we have two scalar meson fields σ and ϕ , which do not contain spin and isospin indices but hold VEVs. Therefore, we parameterize σ and ϕ as

$$\sigma = f_\pi (1 + \bar{\sigma}(r)), \quad (4.58a)$$

$$\phi = \phi_{\text{vac}} (1 + \bar{\phi}(r)), \quad (4.58b)$$

where $\bar{\sigma}(r)$ and $\bar{\phi}(r)$ are dimensionless functions.

Substituting Eqs. (4.27) and (4.58) into the Lagrangian (4.46), the equations of motion for the profile functions $F(r)$, $G(r)$, $W(r)$, $\bar{\sigma}(r)$, and $\bar{\phi}(r)$ are obtained. Detailed expressions are given in Appendix B.

The boundary conditions for the pion, rho, and omega mesons are given in (4.28). The boundary conditions for the scalar mesons are determined as follows: (i) when $r \rightarrow \infty$, both $\bar{\sigma}(r)$ and $\bar{\phi}(r)$ must vanish to reproduce VEVs of the scalar meson fields, i.e.,

$$\bar{\sigma}(\infty) = 0, \quad \bar{\phi}(\infty) = 0 \quad (4.59)$$

and (ii) when $r \rightarrow 0$, the second-order derivatives $\bar{\sigma}''$ and $\bar{\phi}''$ should be nonsingular. The last term in each of Eqs. (B.6) and (B.7) show that

$$\bar{\sigma}'(0) = 0, \quad \bar{\phi}'(0) = 0. \quad (4.60)$$

By taking a functional derivative of the total Lagrangian (4.46) with respect to \mathcal{V}_μ , we obtain the baryon number current. Here, \mathcal{V}_μ represents the $U(1)$ external

gauge field corresponding to the baryon number. After an explicit calculation, we obtain the time component of the baryon number density j_0 as

$$\begin{aligned}
j_0 = & -\frac{2}{3gr^2} \left\{ f_\pi^2 g^2 r^2 a_{\text{hls}} W [s_0 \bar{\sigma}^2 + 2s_0 \bar{\sigma} + 1] \right. \\
& + F' \left[\alpha_2 - 2G(-\alpha_2 + \alpha_3 + \alpha_2 \cos F) + \alpha_2 \cos^2 F \right. \\
& \quad \left. \left. - 2\alpha_2 \cos F + (\alpha_2 - \alpha_3) G^2 \right] \right. \\
& \left. - 2\alpha_3 \sin F G' + \alpha_1 \sin^2 F F' \right\} - \frac{\sin^2 F}{2\pi^2 r^2} F', \quad (4.61)
\end{aligned}$$

where α_1 , α_2 , and α_3 are combinations of c_1 , c_2 , and c_3 given in Eq. (B.2). The baryon number density could be simplified using the equation of motion for W in Eq. (B.5)

$$j_0 = \frac{1}{r^2} \frac{d}{dr} \left(\frac{4\alpha_3 \sin F (\cos F - G - 1)}{3g} - \frac{2r^2 W'}{3g} + \frac{\sin(2F)}{8\pi^2} - \frac{F}{4\pi^2} \right), \quad (4.62)$$

which is consistent with that obtained in Ref.^[59]. Note that by combining the baryon number current (4.62) and the boundary condition (4.28), N_B is obtained as

$$\begin{aligned}
N_B &= \int_0^\infty d^3r j_0(r) \\
&= 4\pi \left(\frac{4\alpha_3 \sin F (\cos F - G - 1)}{3g} - \frac{2r^2 W'}{3g} + \frac{\sin(2F)}{8\pi^2} - \frac{F}{4\pi^2} \right) \Big|_{r \rightarrow 0}^{r \rightarrow \infty} \\
&= 1. \quad (4.63)
\end{aligned}$$

This shows that the baryon number is correctly normalized to one.

In this analysis, the baryon current could be simplified by inserting $c_1 + c_2 = 0$, $c_1 - c_2 = 3/4$, and $c_3 = 0$ into Eq. (4.61):

$$j_0 = -\frac{2}{3gr^2} f_\pi^2 g^2 r^2 a_{\text{hls}} W [s_0 \bar{\sigma}^2 + 2s_0 \bar{\sigma} + 1]. \quad (4.64)$$

In this study, we also investigate the root-mean-square (RMS) radii of the baryon number ($\langle r^2 \rangle_B^{1/2}$) and energy ($\langle r^2 \rangle_E^{1/2}$) densities, which are defined as

$$\begin{aligned}
\langle r^2 \rangle_B^{1/2} &= \sqrt{\int_0^\infty d^3r r^2 j_0(r)}, \\
\langle r^2 \rangle_E^{1/2} &= \sqrt{\frac{1}{M_{\text{sol}}} \int_0^\infty d^3r r^2 \mathcal{M}_{\text{sol}}(r)}, \quad (4.65)
\end{aligned}$$

Quantity	Values
f_π	92.4 MeV
m_π	139.57 MeV
N_c	3
$c_1 + c_2$	0
$c_1 - c_2$	$-4/3$
c_3	0
g	5.80 ± 0.91
a_{hls}	2.07 ± 0.33

Table 4.3: Parameters of the model

where M_{sol} and $\mathcal{M}_{\text{sol}}(r)$ are the skyrmion mass and the corresponding energy density, respectively. They are given in Eq. (B.1).

In this study, the parameters are determined from low energy experiments. In Table 4.3, we summarize the parameters of the model.

4.3.3 Effects of scalar mesons when $A = 0$

In this subsection, we study the effects of scalar mesons on skyrmion properties when $A = 0$. From Eq. (4.47), we observe that when $A = 0$, ϕ only has a trivial solution. Therefore, the scalar meson is a pure two-quark state. In this case, the Lagrangian (4.46) is reduced to

$$\begin{aligned} \mathcal{L} = & \frac{1}{2} \partial_\mu \sigma \partial^\mu \sigma + \sigma^2 \text{Tr}(\alpha_{\perp\mu} \alpha_{\perp}^\mu) \\ & - (V_\sigma - \bar{V}_\sigma) - (V_{\text{SB}} - \bar{V}_{\text{SB}}) + \mathcal{L}_V, \end{aligned} \quad (4.66)$$

where $V_\sigma = \frac{1}{8} \lambda \sigma^4 - \frac{1}{2} m_2^2 \sigma^2$. The parameters λ and m_2^2 determine the masses of σ and π through

$$\begin{aligned} m_\sigma^2 &= -m_2^2 + \frac{3}{2} \lambda f_\pi^2, \\ m_\pi^2 &= -m_2^2 + \frac{1}{2} \lambda f_\pi^2. \end{aligned} \quad (4.67)$$

Here, m_σ denotes the scalar meson mass. In the following discussions, we treat m_σ and s_0 as free parameters of the model and study the effect of these two parameters on skyrmion properties.

Effects of the parameter m_σ on skyrmion properties

To study the effects of the parameter m_σ , we keep s_0 constant, $s_0 = 0$. In this case, the vector meson part is the standard HLS Lagrangian (3.57). We plot the

m_σ dependence of the skyrmion mass and radii in Fig. 4.3.

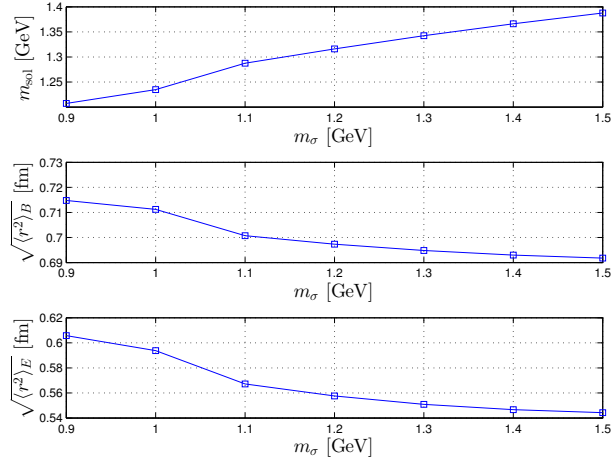


Figure 4.3: m_σ dependence of the skyrmion mass and radii with $A = s_0 = 0$

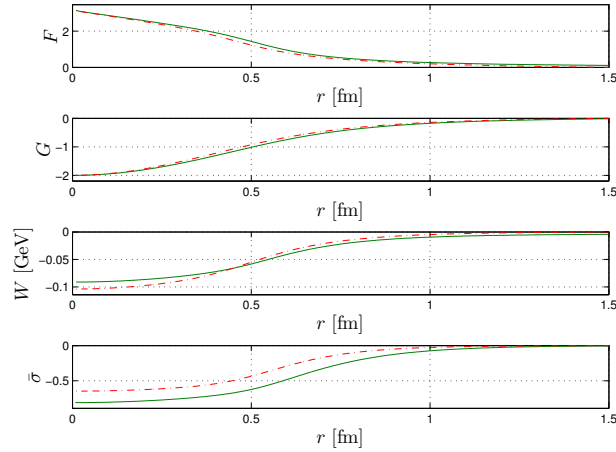


Figure 4.4: m_σ dependence of the profile functions with $A = s_0 = 0$ for $m_\sigma = 1$ GeV (green curve) and $m_\sigma = 1.4$ GeV (red dash-dotted line)

In Fig. 4.3 we show the m_σ dependence of the skyrmion mass m_{sol} and the RMS radii $\sqrt{\langle r^2 \rangle_B}$ and $\sqrt{\langle r^2 \rangle_E}$. In Fig. 4.4 we show the profile functions for several values of m_σ .

As shown in Fig. 4.3, when the magnitude of m_σ increases, the skyrmion mass m_{sol} increases. This tendency can be understood from the profile function of $\bar{\sigma}$ in Fig. 4.4: when the scalar meson mass m_σ is heavy, the magnitude of $\bar{\sigma}$ decreases. Because $\bar{\sigma} < 0$ as m_σ increases, the magnitude of $\sigma = f_\pi(1 + \bar{\sigma})$ becomes large.

Consequently, the contribution of $\sigma^2 \text{Tr}(\alpha_{\perp\mu}\alpha_{\perp}^{\mu})$ to the skyrmion mass (4.46) becomes large. The physical explanation is that when the scalar meson mass m_{σ} is larger, the attractive force produced by the scalar meson is suppressed. Therefore, the skyrmion mass is larger.

In addition, from Fig. 4.3, we observe that when m_{σ} is large, the RMS radii $\sqrt{\langle r^2 \rangle_E}$ and $\sqrt{\langle r^2 \rangle_B}$ are both small. This tendency can be understood from the profile functions in Fig. 4.4. When m_{σ} becomes heavy, the profile for $\bar{\sigma}$ becomes narrow. Physically, the scalar meson σ provides an attractive force, whereas the vector meson ω provides a repulsive force. When σ becomes narrow, the corresponding ω needs to be narrow to maintain the balance between the attractive and repulsive forces. From the expression for the skyrmion mass, (B.1), we observe that the shape of energy distribution is dominated by the shape of the σ and ω . Thus, the narrow σ and ω correspond to a small RMS radius $\sqrt{\langle r^2 \rangle_E}$.

Next, we investigate the radius of baryon number density $\sqrt{\langle r^2 \rangle_B}$. From Eq. (4.64), we observe that when $s_0 = 0$, the profile of the baryon number density is proportional to the profile of the omega meson W . Therefore, a narrow W corresponds to a small radius $\sqrt{\langle r^2 \rangle_B}$. Physically speaking, when m_{σ} is large, the effective ranges of the attractive and repulsive forces provide by σ and ω , respectively, are suppressed. As a result, the skyrmion size $\sqrt{\langle r^2 \rangle_B}$ is small.

Effects of the parameter s_0 on skyrmion properties

From Eq. (4.56), we observe that the chiral invariant vector meson mass is controlled by the parameter s_0 . Here, we investigate the effects of s_0 on skyrmion properties by keeping the scalar meson mass at a typical value $m_{\sigma} = 1.37$ GeV. We plot the s_0 dependence of the skyrmion mass and radii in Fig. 4.5.

From Fig. 4.5, we observe that a high value of s_0 corresponds to a heavy m_{sol} and a broad $\sqrt{\langle r^2 \rangle_B}$. As shown in Eq. (4.56), $a_{\text{hls}}g_{\omega}^2 (f_{\pi}^2(1 - s_0) + s_0\sigma^2(r))$ plays the role of the effective vector mesons mass inside the soliton. From the profile functions shown in Fig. 4.6, we observe that $-1 < \bar{\sigma}(r) \leq 0$, therefore $\sigma(r) \leq f_{\pi}$. As a result, the effective vector meson mass is smaller than the value of the vector meson mass $m_{\omega} = \sqrt{a_{\text{hls}}}g_{\omega}f_{\pi}$ in vacuum. This causes two effects: (i) For a large s_0 , the effective strength of the repulsive force supplied by the ω meson is strong. In the present analysis, the soliton energy is dominated by the vector mesons, therefore a large s_0 corresponds to a large skyrmion mass. (ii) For a large s_0 , the effective range of the repulsive force generated by ω is long. Because the ω meson is the gauge boson of the $U(1)_{\text{V}}$ baryon number symmetry, a large s_0 causes the RMS radius of the baryon number density $\sqrt{\langle r^2 \rangle_B}$ to be large. There is an alternative explanation for the relation between s_0 and $\sqrt{\langle r^2 \rangle_B}$. As shown in Eq. (4.64), the baryon number density is determined from both ω and σ . When s_0 is large, the magnitude of the ω profile function is broad to maintain

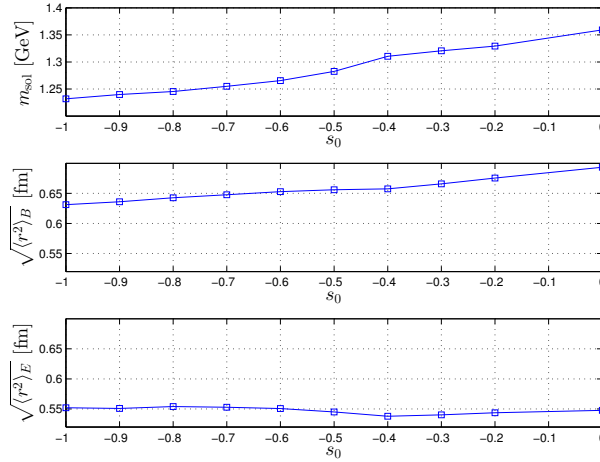


Figure 4.5: s_0 dependence of the skyrmion mass and radii for $m_\sigma = 1.37$ GeV

the conservation of baryon number (4.63). Consequently, the RMS radius of the baryon number density $\sqrt{\langle r^2 \rangle_B}$ is large.

Next we investigate the s_0 dependence of the RMS radius of the energy density $\sqrt{\langle r^2 \rangle_E}$. The numerical error for the present analysis is approximately 1-3%; thus, from the third graph in Fig. 4.6 we conclude that the RMS radius $\sqrt{\langle r^2 \rangle_E}$ is not sensitive to the changes in s_0 . This result implies that the contributions of ω and σ cancel each other.

4.3.4 Effects of scalar mesons when $A \neq 0$

In this subsection, we investigate the scalar meson mixing effect on skyrmion properties when $A \neq 0$. For the present purpose, we fixed two values of s_0 , i.e., $s_0 = 0$ and $s_0 = -0.5$, and treat the mixing angle θ as a free parameter to study the mixing effect on the mass and radii of the skyrmion. The mixing angle θ is defined in Eq. (4.53).

In Figs. 4.7 and 4.8 we show the main numerical results.

From Figs. 4.7 and 4.8, we observe that the decreasing and increasing tendencies of the mass and RMS radii are the same. From Eq. (4.53), we read that a larger $\cos(\theta)$ corresponds to a lighter “effective mass” of the two-quark component scalar meson and a larger magnitude of the two-quark component included in f_{500} . If we compare the “effective mass” of the two-quark component scalar meson and the m_σ shown in Fig. 4.3, we conclude that their tendencies are the same, i.e., the large $\cos \theta$ in Figs. 4.7 and 4.8 corresponds to the small mass m_σ in Fig. 4.3.

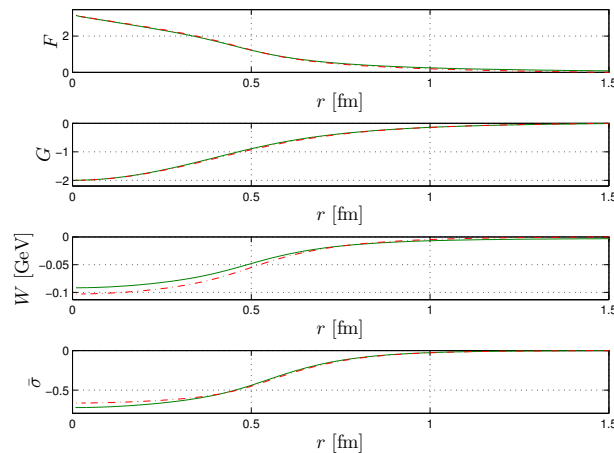


Figure 4.6: Profile functions with $s_0 = -0.5$ (green curve) and $s_0 = 0$ (red dash-dotted line)

From Figs. 4.7 and 4.8, we observe that the solution disappears in the regions of $\cos \theta > 0.6$ when $s_0 = 0$ and $\cos \theta > 0.25$ when $s_0 = -0.5$, i.e., the small s_0 corresponds to a small maximal value of $\cos \theta$. We can understand this fact as follows. From Eq. (4.53) we observe that a large value of $\cos \theta$ means that f_{500} includes a large magnitude of the two-quark component, or equivalently a strong attractive force provide by the scalar meson. In the present analysis, keeping s_0 constant means that the total repulsive force does not change and adjusting $\cos \theta$ means that we adjust the total attractive force. Because the soliton collapses when the total attractive force is larger than the total repulsive force, the soliton survives for a certain range of $\cos \theta$. For the parameter s_0 , a small s_0 means that a weak repulsive force is provided by the ω meson, as we stated above. As a result, a small s_0 corresponds to a narrow range of $\cos \theta$.

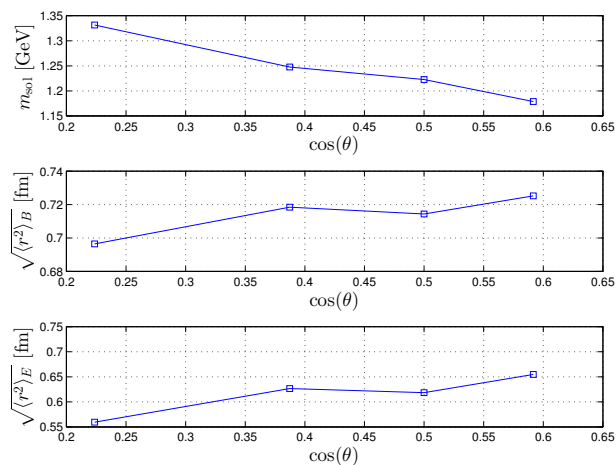


Figure 4.7: Dependence of skyrmin properties on the mixing angle between two scalar mesons for $s_0 = 0$

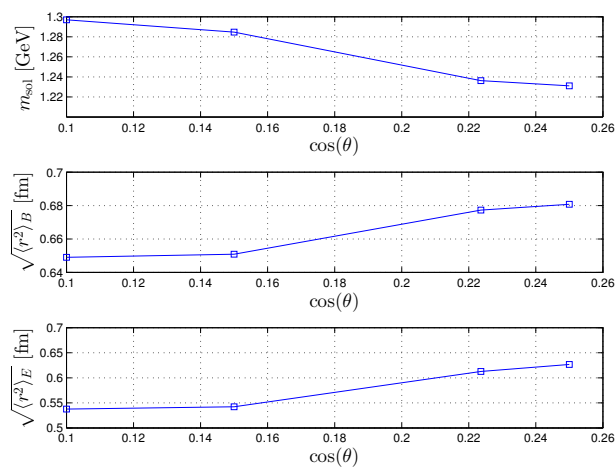


Figure 4.8: Dependence of skyrmin properties on the mixing angle between two scalar mesons for $s_0 = -0.5$

Chapter 5

Discussion and Conclusion

In this thesis, we first reviewed the basic QCD properties and then two chiral effective models to describe meson properties in the low energy region. Then we investigated the baryon properties through meson dynamics in the Skyrme approach.

We found that the skyrmion constructed in an effective meson model containing the pion, rho, and omega mesons has the critical problem that the mass of the skyrmion is approximately 50% heavier than the lightest physical baryon state. To solve this problem, we constructed an effective model that includes the pion, rho, and omega mesons together with two- and four-quark scalar mesons.

First, we switched off the mixing between the two- and four-quark scalar meson fields. In this case, the pure four-quark meson decouples from the other mesons. We investigated the effect of the mass of the two-quark scalar meson on skyrmion properties and found that when the mass of the scalar meson becomes light the skyrmion mass becomes light, whereas the root-mean-square radii of the baryon number density $\sqrt{\langle r^2 \rangle_B}$ and the energy density $\sqrt{\langle r^2 \rangle_E}$ become large. We then investigated the effect of coupling between scalar and vector mesons on skyrmion properties. The result shows that when the coupling is large, the skyrmion mass and radii are large. We finally switched on the mixing between the two-quark and four-quark scalar mesons, and investigated skyrmion properties. We found that when the lighter scalar meson contains a larger percentage of the two-quark component, the skyrmion mass is smaller, and the RMS radii ($\sqrt{\langle r^2 \rangle_B}$ and $\sqrt{\langle r^2 \rangle_E}$) are larger.

The results obtained from previous studies and our current findings are summarized in Tables 5.1 and 5.2. From Table 5.1, we observe that the mass and radius of the soliton depend on how the scalar meson is introduced. From Table 5.2, we observe that at the leading order, the mass and radius of the soliton obtained from the present analysis are closer to the experimental values.

Table 5.1: The parameter dependence of mass and radius of the skyrmion (\diamond 's denote the previous analysis and \blacklozenge 's denote the present analysis.)

	model	scalar type	parameter	soliton mass [MeV]	$\sqrt{\langle r^2 \rangle_B}$ [fm]
\diamond	$\pi\sigma$ ^[19]	2 quark	m_σ (\nearrow)	\nearrow	\searrow
\diamond	$\pi\rho\omega\chi$ ^[20]	glueball	m_χ (\nearrow)	\nearrow	\searrow
\blacklozenge	$\pi\rho\omega\sigma$ ^[55]	2 quark	m_σ (\nearrow)	\nearrow	\searrow
\blacklozenge	$\pi\rho\omega\sigma$ ^[55]	2 quark	s_0 (\nearrow)	\nearrow	\nearrow
\blacklozenge	$\pi\rho\omega\sigma\phi$ ^[55]	2 + 4 quark	$\cos\theta$ (\nearrow)	\searrow	\nearrow

Table 5.2: The mass and radius of the skyrmion from the leading order (\diamond 's denote the previous analysis and \blacklozenge denotes the present analysis)

	model	scalar type	parameter	soliton mass	$\sqrt{\langle r^2 \rangle_B}$
	Experiment	-	-	939 MeV	0.72 fm
\diamond	π ^[19]	-	-	1756.5 MeV	0.51 fm
\diamond	$\pi\sigma$ ^[19]	2 quark	$m_\sigma = 560$ MeV	1364.5 MeV	0.56 fm
\diamond	$\pi\rho\omega$ ^[20]	-	-	1469.0 MeV	0.49 fm
\diamond	$\pi\rho\omega\chi$ ^[20]	glueball	$m_\chi = 720$ MeV	1408.3 MeV	0.51 fm
\blacklozenge	$\pi\rho\omega\sigma\phi$ ^[55]	2 + 4 quark	$\cos\theta = 0.6$ ^[27]	1180 MeV	0.72 fm

Table 5.3: The mass and radius of the skyrmion from the $\mathcal{O}(p^4)$ terms of HLS

model	scalar type	parameter	soliton mass	$\sqrt{\langle r^2 \rangle_B}$
$\pi\rho\omega$ ^[25]	-	-	1188.8 MeV	0.43 fm
$\pi\rho\omega\chi$ ^[25]	glueball	$m_\chi = 720$ MeV	1138.0 MeV	0.43 fm

The present study shows that, even though both the two-quark and four-quark scalar mesons are included, the skyrmion mass is still approximately 300 MeV larger than the lightest nucleon mass. In Ref.^[25], it was shown that the $\mathcal{O}(p^4)$ terms of HLS also modify the mass and size of the skyrmion, as in Table 5.3. Therefore, to reproduce the baryon and meson properties in a single model, we need to extend the model by including, e.g., another scalar meson as a dilaton, $\mathcal{O}(p^4)$ terms of HLS for the vector mesons^[25], and so on. We leave these studies as future projects.

Acknowledgments

I would like to thank my adviser, Professor Masayasu Harada for introducing me to research in hadron physics, and for his encouragement, patience, and expert suggestions. I also want to thank Professors Yong-liang Ma, Chiho Nonaka, and Shinya Matsuzaki, who have given me much valuable advise inside and outside of physics.

I would like to thank Mr. Hiroki Nishihara and Mr. Yuichi Motohiro for their wise discussions while writing this thesis.

During the last six years of my stay in Japan, I received a lot of help from the EHQG group members. Without their help, I would not have been able to live and study in Japan. I will remember your kindness the rest of my life.

Of course, my education would not have been possible without the support and understanding of my parents. I am sorry for having been apart from you for such a long time.

My work has been supported in part by the Nagoya University Program for Leading Graduate Schools “Leadership Development Program for Space Exploration and Research.”

Appendix A

The mass mixing matrix for the scalar meson

The masses of f_{500} and f_{1370} are expressed as

$$m_{f_{500}}^2 = \frac{1}{2} \left(-\sqrt{2f_\pi^2 (4A^2 - \lambda m_4^2 + \lambda m_\pi^2) + f_\pi^4 \lambda^2 + (m_4^2 - m_\pi^2)^2} + f_\pi^2 \lambda + m_4^2 + m_\pi^2 \right), \quad (\text{A.1})$$

$$m_{f_{1370}}^2 = \frac{1}{2} \left(\sqrt{2f_\pi^2 (4A^2 - \lambda m_4^2 + \lambda m_\pi^2) + f_\pi^4 \lambda^2 + (m_4^2 - m_\pi^2)^2} + f_\pi^2 \lambda + m_4^2 + m_\pi^2 \right). \quad (\text{A.2})$$

The mixing angle θ is obtained as

$$\theta = \arctan \sqrt{\frac{m_{f_{1370}}^2 - m_4^2}{m_4^2 - m_{f_{500}}^2}} = \arccos \sqrt{\frac{m_4^2 - m_{f_{500}}^2}{m_{f_{1370}}^2 - m_{f_{500}}^2}}. \quad (\text{A.3})$$

From Eqs. (4.48), (4.49), (A.1), and (A.2), one gets

$$\begin{aligned} A^2 &= \frac{(m_{f_{1370}}^2 - m_4^2)(m_4^2 - m_{f_{500}}^2)}{2f_\pi^2}, \\ \lambda &= \frac{m_{f_{500}}^2 + m_{f_{1370}}^2 - m_4^2 - m_\pi^2}{f_\pi^2}, \\ \phi_{\text{vac}} &= -\frac{Af_\pi^2}{\sqrt{2}m_4^2}, \\ m_2^2 &= \frac{1}{2} \left(\frac{m_{f_{500}}^2 m_{f_{1370}}^2}{m_4^2} - 3m_\pi^2 \right), \end{aligned} \quad (\text{A.4})$$

with $m_{f_{500}}^2 < m_4^2 < m_{f_{1370}}^2$.

Appendix B

Skyrmion mass and the equations of motion for the profile functions $F(r)$, $G(r)$, $W(r)$, $\bar{\sigma}(r)$, and $\bar{\phi}(r)$

Substituting the ansatz Eqs. (4.27) and (4.58) into the Lagrangian (4.46), we obtain the skyrmion mass as

$$\begin{aligned}
M_{\text{sol}} &= 4\pi \int_0^\infty dr r^2 \mathcal{M}_{\text{sol}}(r) \\
&= -4\pi \int_0^\infty dr \left\{ \frac{1}{8} r^2 \left\{ 4f_\pi^2 g^2 s_0 a_{\text{hls}} W^2 \bar{\sigma}(\bar{\sigma} + 2) - 4f_\pi^2 (\bar{\sigma} + 1)^2 F'^2 \right. \right. \\
&\quad + f_\pi^2 \left[\frac{2(m_4^2 - m_{f_{500}}^2)(m_{f_{1370}}^2 - m_4^2)(\bar{\sigma} + 1)^2 (\bar{\phi} + 1)}{m_4^2} \right. \\
&\quad - (m_{f_{500}}^2 + m_{f_{1370}}^2 - m_4^2 - m_\pi^2)(\bar{\sigma} + 1)^4 \\
&\quad + \frac{2(m_{f_{500}}^2 m_{f_{1370}}^2 - 3m_4^2 m_\pi^2)(\bar{\sigma} + 1)^2}{m_4^2} \\
&\quad + \frac{(m_4^2 - m_{f_{500}}^2)(m_4^2 - m_{f_{1370}}^2)(\bar{\phi} + 1)^2}{m_4^2} + 8m_\pi^2 (\bar{\sigma} + 1) \cos(F) \left. \right] \\
&\quad + \frac{f_\pi^2 (m_4^2 - m_{f_{500}}^2)(m_4^2 - m_{f_{1370}}^2) \bar{\phi}^2}{m_4^4} - 4f_\pi^2 \bar{\sigma}'^2 + 4f_\pi^2 g^2 a_{\text{hls}} W^2 \\
&\quad \left. - \frac{f_\pi^2 (m_{f_{500}}^2 m_{f_{1370}}^2 + 3m_4^2 m_\pi^2)}{m_4^2} + 4W'^2 \right\} \\
&\quad - \frac{1}{2g^2} \left\{ 8f_\pi^2 g^2 a_{\text{hls}} G \sin^2 \left(\frac{F}{2} \right) (s_0 \bar{\sigma}^2 + 2s_0 \bar{\sigma} + 1) \right.
\end{aligned}$$

$$\begin{aligned}
& -4f_\pi^2 g^2 \bar{\sigma}^2 \sin^2\left(\frac{F}{2}\right) ((s_0 a_{\text{hls}} - 1) \cos(F) - s_0 a_{\text{hls}} - 1) \\
& -8f_\pi^2 g^2 \bar{\sigma} \sin^2\left(\frac{F}{2}\right) ((s_0 a_{\text{hls}} - 1) \cos(F) - s_0 a_{\text{hls}} - 1) \\
& +2f_\pi^2 g^2 a_{\text{hls}} G^2 (s_0 \bar{\sigma}^2 + 2s_0 \bar{\sigma} + 1) \\
& +8f_\pi^2 g^2 a_{\text{hls}} \sin^4\left(\frac{F}{2}\right) - f_\pi^2 g^2 \cos(2F) + f_\pi^2 g^2 + 2G'^2 \} \\
& -\alpha_3 \left(2G (WF' - \sin(F)W') + G^2 WF' \right. \\
& \quad \left. + 2 \sin(F) ((\cos(F) - 1)W' + WG') \right) \\
& +\alpha_2 WF' (-\cos(F) + G + 1)^2 \\
& +\alpha_1 WF' \sin^2(F) - \frac{G^2(G+2)^2}{2g^2 r^2} \}, \tag{B.1}
\end{aligned}$$

with

$$\alpha_1 = \frac{3gN_c}{16\pi^2} (c_1 - c_2), \alpha_2 = \frac{gN_c}{16\pi^2} (c_1 + c_2), \alpha_3 = \frac{gN_c}{16\pi^2} c_3. \tag{B.2}$$

The equations of motion for $F(r)$, $G(r)$, $W(r)$, $\bar{\sigma}(r)$, and $\bar{\phi}(r)$ are

$$\begin{aligned}
F'' &= \frac{1}{f_\pi^2 r^2 (1 + \bar{\sigma})^2} \\
&\times \left\{ 2G (f_\pi^2 s_0 a_{\text{hls}} \bar{\sigma}^2 \sin F + 2f_\pi^2 s_0 a_{\text{hls}} \bar{\sigma} \sin F + f_\pi^2 a_{\text{hls}} \sin F \right. \\
&\quad - \alpha_2 \cos F W' - \alpha_3 \cos F W' + (\alpha_2 - \alpha_3)(WG' + W')) \\
&\quad - f_\pi^2 \bar{\sigma} \sin F (4s_0 a_{\text{hls}} \cos F - 4s_0 a_{\text{hls}} - 4 \cos F - r^2 m_\pi^2) \\
&\quad - 2f_\pi^2 \bar{\sigma}^2 \sin F (s_0 a_{\text{hls}} \cos F - s_0 a_{\text{hls}} - \cos F) - f_\pi^2 a_{\text{hls}} \sin(2F) \\
&\quad - 2f_\pi^2 r^2 F' \bar{\sigma}' - 2f_\pi^2 r \bar{\sigma}^2 F' - 2f_\pi^2 r \bar{\sigma} F' (r \bar{\sigma}' + 2) + 2f_\pi^2 a_{\text{hls}} \sin F \\
&\quad - 2f_\pi^2 r F' + f_\pi^2 m_\pi^2 r^2 \sin F + f_\pi^2 \sin(2F) \\
&\quad - 2\alpha_2 W \cos F G' + 2\alpha_3 W \cos F G' \\
&\quad - \frac{1}{2} \alpha_1 \cos(2F) W' - 2\alpha_2 \cos F W' + \frac{1}{2} \alpha_2 \cos(2F) W' \\
&\quad - 2\alpha_3 \cos F W' + 2\alpha_3 \cos(2F) W' + 2\alpha_2 W G' \\
&\quad \left. - 2\alpha_3 W G' + (\alpha_2 - \alpha_3) G^2 W' + \frac{1}{2} \alpha_1 W' + \frac{3}{2} \alpha_2 W' \right\}, \tag{B.3}
\end{aligned}$$

$$\begin{aligned}
G'' &= -f_\pi^2 g^2 a_{\text{hls}} (s_0 \bar{\sigma}^2 + 2s_0 \bar{\sigma} + 1) (\cos F - G - 1) \\
&- \alpha_3 g^2 (WF' (\cos F - G - 1) + 2 \sin F W') \\
&+ \alpha_2 g^2 WF' (\cos F - G - 1) + \frac{G(G^2 + 3G + 2)}{r^2}, \tag{B.4}
\end{aligned}$$

$$\begin{aligned}
W'' &= f_\pi^2 g^2 a_{\text{hls}} W (s_0 \bar{\sigma}^2 + 2s_0 \bar{\sigma} + 1) - \frac{2W'}{r} \\
&+ \frac{1}{r^2} \left\{ -\alpha_3 (F' (2G(\cos F + 1) + 2(\cos F - \cos(2F)) + G^2) + 4 \sin F G') \right. \\
&\quad \left. + \alpha_2 F' (-\cos F + G + 1)^2 + 2\alpha_1 F' \sin^2 \left(\frac{F}{2} \right) (\cos F + 1) \right\}, \quad (\text{B.5})
\end{aligned}$$

$$\begin{aligned}
\bar{\sigma}'' &= \frac{1}{2m_4^2} \left\{ m_4^2 (2\bar{\sigma} (-g^2 s_0 a_{\text{hls}} W^2 + m_{f_{500}}^2 + m_{f_{1370}}^2 + F'^2 - m_4^2)) \right. \\
&\quad + (m_{f_{500}}^2 + m_{f_{1370}}^2 - m_4^2 - m_\pi^2) \bar{\sigma}^3 + 3 (m_{f_{500}}^2 + m_{f_{1370}}^2 - m_4^2 - m_\pi^2) \bar{\sigma}^2 \\
&\quad + 2 [-g^2 s_0 a_{\text{hls}} W^2 + F'^2 - m_\pi^2 (\cos F - 1)] \\
&\quad \left. - (m_4^2 - m_{f_{500}}^2) (m_{f_{1370}}^2 - m_4^2) (\bar{\sigma} + 1) \bar{\phi} \right\} \\
&\quad - \frac{(\bar{\sigma} + 1) (-8s_0 a_{\text{hls}} (G \sin^2 (\frac{F}{2}) + \sin^4 (\frac{F}{2})) - 2s_0 a_{\text{hls}} G^2 + \cos(2F) - 1)}{r^2} \\
&\quad - \frac{2\bar{\sigma}'}{r}, \quad (\text{B.6})
\end{aligned}$$

$$\bar{\phi}'' = m_4^2 (\bar{\phi} - \bar{\sigma} (\bar{\sigma} + 2)) - \frac{2\bar{\phi}'}{r}. \quad (\text{B.7})$$

References

- [1] G. E. Brown and Mannque Rho. Chiral restoration in hot and/or dense matter. Phys. Rept., 269:333–380, 1996. arXiv:hep-ph/9504250, doi:10.1016/0370-1573(95)00067-4.
- [2] Craig D. Roberts and Sebastian M. Schmidt. Dyson-Schwinger equations: Density, temperature and continuum strong QCD. Prog. Part. Nucl. Phys., 45:S1–S103, 2000. arXiv:nucl-th/0005064, doi:10.1016/S0146-6410(00)90011-5.
- [3] Mark G. Alford, Andreas Schmitt, Krishna Rajagopal, and Thomas Schäfer. Color superconductivity in dense quark matter. Rev. Mod. Phys., 80:1455–1515, 2008. arXiv:0709.4635, doi:10.1103/RevModPhys.80.1455.
- [4] Kenji Fukushima and Tetsuo Hatsuda. The phase diagram of dense QCD. Rept. Prog. Phys., 74:014001, 2011. arXiv:1005.4814, doi:10.1088/0034-4885/74/1/014001.
- [5] Krishna Rajagopal and Frank Wilczek. Static and dynamic critical phenomena at a second order QCD phase transition. Nucl. Phys., B399:395–425, 1993. arXiv:hep-ph/9210253, doi:10.1016/0550-3213(93)90502-G.
- [6] F. Karsch. Lattice QCD at high temperature and density. Lect. Notes Phys., 583:209–249, 2002. arXiv:hep-lat/0106019, doi:10.1007/3-540-45792-5_6.
- [7] C.R. Allton, S. Ejiri, S.J. Hands, O. Kaczmarek, F. Karsch, et al. The QCD thermal phase transition in the presence of a small chemical potential. Phys. Rev., D66:074507, 2002. arXiv:hep-lat/0204010, doi:10.1103/PhysRevD.66.074507.

- [8] Michael Buballa. NJL model analysis of quark matter at large density. Phys. Rept., 407:205–376, 2005. arXiv:hep-ph/0402234, doi:10.1016/j.physrep.2004.11.004.
- [9] Y. Aoki, Szabolcs Borsanyi, Stephan Durr, Zoltan Fodor, Sandor D. Katz, et al. The QCD transition temperature: results with physical masses in the continuum limit II. JHEP, 0906:088, 2009. arXiv:0903.4155, doi:10.1088/1126-6708/2009/06/088.
- [10] Igor R. Klebanov. Nuclear Matter in the Skyrme Model. Nucl. Phys., B262:133, 1985. doi:10.1016/0550-3213(85)90068-9.
- [11] Hee-Jung Lee, Byung-Yoon Park, Dong-Pil Min, Mannque Rho, and Vicente Vento. A Unified approach to high density: Pion fluctuations in skyrmion matter. Nucl. Phys., A723:427–446, 2003. arXiv:hep-ph/0302019, doi:10.1016/S0375-9474(03)01452-0.
- [12] T. H. R. Skyrme. A Unified Field Theory of Mesons and Baryons. Nucl. Phys., 31:556–569, 1962. doi:10.1016/0029-5582(62)90775-7.
- [13] Gerald E. Brown and Mannque Rho. The Multifaceted Skyrmion. 2009. arXiv:0907.1963.
- [14] T. Fujiwara, Y. Igarashi, A. Kobayashi, H. Otsu, T. Sato, and S. Sawada. An Effective Lagrangian for Pions, ρ Mesons and Skyrmions. Prog. Theor. Phys., 74:128, 1985. doi:10.1143/PTP.74.128.
- [15] Y. Igarashi, M. Johmura, A. Kobayashi, H. Otsu, T. Sato, and S. Sawada. Stabilization of Skyrmions via ρ Mesons. Nucl. Phys., B259:721–729, 1985. doi:10.1016/0550-3213(85)90010-0.
- [16] U. G. Meissner and I. Zahed. Skyrmions in the Presence of Vector Mesons. Phys. Rev. Lett., 56:1035, 1986. doi:10.1103/PhysRevLett.56.1035.
- [17] Ulf G. Meissner, Norbert Kaiser, Andreas Wirzba, and Wolfram Weise. Skyrmions With ρ and ω Mesons as Dynamical Gauge Bosons. Phys. Rev. Lett., 57:1676, 1986. doi:10.1103/PhysRevLett.57.1676.
- [18] I. Zahed and G. E. Brown. The Skyrme Model. Phys. Rept., 142:1–102, 1986. doi:10.1016/0370-1573(86)90142-0.

- [19] F. L. Braghin and I. P. Cavalcante. The Skyrmion model and the dynamical breakdown of chiral symmetry. *Phys. Rev.*, C67:065207, 2003.
arXiv:hep-ph/0304054,
doi:10.1103/PhysRevC.67.065207.
- [20] Byung-Yoon Park, Mannque Rho, and Vicente Vento. Vector mesons and dense Skyrmion matter. *Nucl. Phys.*, A736:129–145, 2004.
arXiv:hep-ph/0310087,
doi:10.1016/j.nuclphysa.2004.01.131.
- [21] Ralf Rapp and Edward V. Shuryak. Thermal dilepton radiation at intermediate masses at the CERN - SPS. *Phys. Lett.*, B473:13–19, 2000.
arXiv:hep-ph/9909348,
doi:10.1016/S0370-2693(99)01367-2.
- [22] Hee-Jung Lee, Byung-Yoon Park, Mannque Rho, and Vicente Vento. Sliding vacua in dense skyrmion matter. *Nucl. Phys.*, A726:69–92, 2003.
arXiv:hep-ph/0304066,
doi:10.1016/S0375-9474(03)01626-9.
- [23] Byung-Yoon Park, Mannque Rho, and Vicente Vento. The Role of the Dilaton in Dense Skyrmion Matter. *Nucl. Phys.*, A807:28–37, 2008.
arXiv:0801.1374,
doi:10.1016/j.nuclphysa.2008.03.015.
- [24] Byung-Yoon Park and Vicente Vento. Skyrmion approach to finite density and temperature. 2009. arXiv:0906.3263.
- [25] Yong-Liang Ma, Masayasu Harada, Hyun Kyu Lee, Yongseok Oh, Byung-Yoon Park, and Mannque Rho. Dense baryonic matter in conformally-compensated hidden local symmetry: Vector manifestation and chiral symmetry restoration. *Phys. Rev.*, D90(3):034015, 2014.
arXiv:1308.6476, doi:10.1103/PhysRevD.90.034015.
- [26] A. Chodos, R. L. Jaffe, K. Johnson, Charles B. Thorn, and V. F. Weisskopf. A New Extended Model of Hadrons. *Phys. Rev.*, D9:3471–3495, 1974.
doi:10.1103/PhysRevD.9.3471.
- [27] Amir H. Fariborz, Renata Jora, and Joseph Schechter. Global aspects of the scalar meson puzzle. *Phys. Rev.*, D79:074014, 2009.
arXiv:0902.2825, doi:10.1103/PhysRevD.79.074014.

- [28] Daisuke Jido, Makoto Oka, and Atsushi Hosaka. Chiral symmetry of baryons. Prog. Theor. Phys., 106:873–908, 2001.
arXiv:hep-ph/0110005, doi:10.1143/PTP.106.873.
- [29] Mark G. Alford, Krishna Rajagopal, and Frank Wilczek. QCD at finite baryon density: Nucleon droplets and color superconductivity. Phys. Lett., B422:247–256, 1998. arXiv:hep-ph/9711395,
doi:10.1016/S0370-2693(98)00051-3.
- [30] R. Rapp, Thomas Schafer, Edward V. Shuryak, and M. Velkovsky. Diquark Bose condensates in high density matter and instantons. Phys. Rev. Lett., 81:53–56, 1998. arXiv:hep-ph/9711396,
doi:10.1103/PhysRevLett.81.53.
- [31] Bing-Ran He and Masayasu Harada. Parity doubling structure of nucleon at nonzero density in the holographic mean field theory. Phys. Rev., D88(9):095007, 2013. arXiv:1304.7866,
doi:10.1103/PhysRevD.88.095007.
- [32] Yoichiro Nambu and G. Jona-Lasinio. DYNAMICAL MODEL OF ELEMENTARY PARTICLES BASED ON AN ANALOGY WITH SUPERCONDUCTIVITY. II. Phys. Rev., 124:246–254, 1961.
doi:10.1103/PhysRev.124.246.
- [33] Tetsuo Hatsuda and Teiji Kunihiro. QCD phenomenology based on a chiral effective Lagrangian. Phys. Rept., 247:221–367, 1994.
arXiv:hep-ph/9401310,
doi:10.1016/0370-1573(94)90022-1.
- [34] M. Cheng, N.H. Christ, S. Datta, J. van der Heide, C. Jung, et al. The QCD equation of state with almost physical quark masses. Phys. Rev., D77:014511, 2008. arXiv:0710.0354,
doi:10.1103/PhysRevD.77.014511.
- [35] J. Gasser and H. Leutwyler. Chiral Perturbation Theory to One Loop. Annals Phys., 158:142, 1984.
doi:10.1016/0003-4916(84)90242-2.
- [36] J. Gasser and H. Leutwyler. Chiral Perturbation Theory: Expansions in the Mass of the Strange Quark. Nucl. Phys., B250:465, 1985.
doi:10.1016/0550-3213(85)90492-4.

- [37] G. Ecker. Chiral perturbation theory. Prog. Part. Nucl. Phys., 35:1–80, 1995. arXiv:hep-ph/9501357, doi:10.1016/0146-6410(95)00041-G.
- [38] G. Ecker, J. Gasser, A. Pich, and E. de Rafael. The Role of Resonances in Chiral Perturbation Theory. Nucl. Phys., B321:311, 1989. doi:10.1016/0550-3213(89)90346-5.
- [39] Stefan Scherer. Introduction to chiral perturbation theory. Adv. Nucl. Phys., 27:277, 2003. arXiv:hep-ph/0210398.
- [40] Stefan Scherer and Matthias R. Schindler. A Chiral perturbation theory primer. 2005. arXiv:hep-ph/0505265.
- [41] Stefan Scherer and Matthias R. Schindler. A Primer for Chiral Perturbation Theory. Lect. Notes Phys., 830:pp.1–338, 2012. doi:10.1007/978-3-642-19254-8.
- [42] J. Gasser, M. E. Sainio, and A. Svarc. Nucleons with Chiral Loops. Nucl. Phys., B307:779, 1988. doi:10.1016/0550-3213(88)90108-3.
- [43] Johan Bijnens. Chiral perturbation theory beyond one loop. Prog. Part. Nucl. Phys., 58:521–586, 2007. arXiv:hep-ph/0604043, doi:10.1016/j.pnnp.2006.08.002.
- [44] J. Wess and B. Zumino. Consequences of anomalous Ward identities. Phys. Lett., B37:95, 1971. doi:10.1016/0370-2693(71)90582-X.
- [45] Edward Witten. Global Aspects of Current Algebra. Nucl. Phys., B223:422–432, 1983. doi:10.1016/0550-3213(83)90063-9.
- [46] J. Bijnens. Chiral perturbation theory and anomalous processes. Int. J. Mod. Phys., A8:3045–3105, 1993. doi:10.1142/S0217751X93001235.
- [47] Masayasu Harada and Koichi Yamawaki. Hidden local symmetry at loop: A New perspective of composite gauge boson and chiral phase transition. Phys. Rept., 381:1–233, 2003. arXiv:hep-ph/0302103, doi:10.1016/S0370-1573(03)00139-X.
- [48] John F. Donoghue, Carlos Ramirez, and German Valencia. The Spectrum of QCD and Chiral Lagrangians of the Strong and Weak Interactions. Phys. Rev., D39:1947, 1989. doi:10.1103/PhysRevD.39.1947.

- [49] M. Bando, T. Kugo, S. Uehara, K. Yamawaki, and T. Yanagida. Is rho Meson a Dynamical Gauge Boson of Hidden Local Symmetry? Phys. Rev. Lett., 54:1215, 1985. doi:10.1103/PhysRevLett.54.1215.
- [50] Masako Bando, Taichiro Kugo, and Koichi Yamawaki. On the Vector Mesons as Dynamical Gauge Bosons of Hidden Local Symmetries. Nucl. Phys., B259:493, 1985. doi:10.1016/0550-3213(85)90647-9.
- [51] Masako Bando, Taichiro Kugo, and Koichi Yamawaki. Nonlinear Realization and Hidden Local Symmetries. Phys. Rept., 164:217-314, 1988. doi:10.1016/0370-1573(88)90019-1.
- [52] Masaharu Tanabashi. Chiral perturbation to one loop including the rho meson. Phys. Lett., B316:534-541, 1993. arXiv:hep-ph/9306237, doi:10.1016/0370-2693(93)91040-T.
- [53] O. Kaymakcalan, S. Rajeev, and J. Schechter. Nonabelian Anomaly and Vector Meson Decays. Phys. Rev., D30:594, 1984. doi:10.1103/PhysRevD.30.594.
- [54] Takanori Fujiwara, Taichiro Kugo, Haruhiko Terao, Shozo Uehara, and Koichi Yamawaki. Nonabelian Anomaly and Vector Mesons as Dynamical Gauge Bosons of Hidden Local Symmetries. Prog. Theor. Phys., 73:926, 1985. doi:10.1143/PTP.73.926.
- [55] Bing-Ran He, Yong-Liang Ma, and Masayasu Harada. Effects of scalar mesons in a Skyrme model with hidden local symmetry. Phys. Rev., D92(7):076007, 2015. arXiv:1507.00437, doi:10.1103/PhysRevD.92.076007.
- [56] Gregory S. Adkins, Chiara R. Nappi, and Edward Witten. Static Properties of Nucleons in the Skyrme Model. Nucl. Phys., B228:552, 1983. doi:10.1016/0550-3213(83)90559-X.
- [57] Gregory S. Adkins and Chiara R. Nappi. Stabilization of Chiral Solitons via Vector Mesons. Phys. Lett., B137:251, 1984. doi:10.1016/0370-2693(84)90239-9.
- [58] U. G. Meissner, Norbert Kaiser, and W. Weise. Nucleons as Skyrme Solitons with Vector Mesons: Electromagnetic and Axial Properties. Nucl. Phys., A466:685, 1987. doi:10.1016/0375-9474(87)90463-5.
- [59] Ulf G. Meissner, Norbert Kaiser, H. Weigel, and J. Schechter. Realistic Pseudoscalar - Vector Lagrangian. 2. Static and Dynamical Baryon

Properties. Phys. Rev., D39:1956–1972, 1989. [Erratum: Phys. Rev.D40,262(1989)]. doi:10.1103/PhysRevD.39.1956.